Early life exercise primes the neural epigenome to facilitate gene expression and hippocampal memory consolidation.

Raus AM*[1], Fuller TD*[2], Nelson NE*[1], Valientes DA[2], Bayat A[2], Ivy AS[1,2,3,4]

[1]Physiology/Biophysics, Anatomy/Neurobiology, University of California- Irvine School of Medicine, Irvine, CA

[2]Pediatrics, University of California- Irvine School of Medicine, Irvine, CA

[3]Neurobiology and Behavior, University of California- Irvine School of Biological Sciences, Irvine, CA

[4]Division of Neurology, Children's Hospital Orange County, Orange, CA

Correspondence to aivy@hs.uci.edu

*These authors contributed equally to the manuscript.

Abstract

Aerobic exercise promotes neuroplasticity and hippocampal memory. In the developing brain, epigenetic modifications resulting from early-life exercise (ELE) has not been fully explored. In this study we employ a line of transgenic mice expressing the NuTRAP (Nuclear tagging and Translating Ribosome Affinity Purification) cassette in Emx1 expressing cells, allowing for the simultaneous isolation of translating mRNA and nuclear chromatin from a hippocampal neuron-enriched cell population. After mice undergo ELE, we perform a novel technique of Simultaneous Isolation of Nuclei TAgged in specific Cell Types (INTACT) and Translating Ribosome Affinity Purification (TRAP) (together: "SIT") from a single hippocampus. Data from RNA- and CUT&RUN-seq were coupled to evaluate histone modifications influencing the expression of translating mRNA in neurons after ELE. We then evaluated new gene expression – histone modification relationships during memory consolidation that are likely critical for facilitated memory after ELE. Our data reveal novel candidate gene-histone modification interactions for further investigation.

Introduction

Environmental experiences engage epigenetic mechanisms to modulate gene expression and cell function in post-mitotic neurons[1,2]. Histone modifications and DNA methylation are particularly important for neuronal adaptation to environmental signals by altering transcription and synaptic function[3,4]. Behavioral outputs such as stress susceptibility, reward seeking, and long-term memory have been shown to result from changes to chromatin accessibility and gene expression in neurons[5-9]. In addition to this, the neuronal chromatin landscape undergoes waves of epigenetic modifications as a function of brain maturation itself[10-12]. Postnatal periods of heightened sensitivity to environmental stimuli can lead to lasting changes to cellular function and may result from temporally specific epigenetic mechanisms in the developing brain[13,14]. Whether gene regulatory mechanisms in postmitotic neurons are uniquely influenced by early-life experiences to inform long-term function is a question that is just beginning to be explored. Identifying epigenetic processes involved in modulating cell function, particularly during brain development, is critical for understanding how early-life experiences impact long-term behavioral outcomes.

Aerobic exercise has generally been found to enhance performance on cognitive tasks involving the hippocampus in both adult humans and animal models[15,16]. The type, timing, and duration of exercise exposure matters with regard to whether it has a persistent impact on hippocampal function[17-19]. However, in general, the effects of exercise on hippocampal memory in adulthood are transient[17-19]. Findings in adult rodents also implicate a role for histone modifying enzymes in the mechanisms of exercise-induced benefits to hippocampal memory. Both voluntary exercise or treatment with a HDAC3 inhibitor enable hippocampal memory after a subthreshold learning stimulus, increase brain-derived neurotrophic factor (BDNF), and promote acetylation of H4K8 at the BDNF promoter[20-22]. This suggests that exercise engages epigenetic regulatory mechanisms to promote plasticity. Adult exercise also opens a temporal window for persistent improvements to memory performance when a reactivating exercise exposure is introduced[23]. This suggests a “molecular memory” of the initial exercise[23]. Although the majority of these studies have been performed in adults, more recent work suggests that the effects of exercise on hippocampal memory and the associated alterations in

63 neurotrophic factor expression, synaptic plasticity, and neurogenesis are similar in
64 juvenile and adolescent periods[17,24-27]. Previous work in our lab showed that early-life
65 exercise (ELE) for either one week (juvenile period; postnatal days (P) 21-27) or three
66 weeks (juvenile-adolescence; P21-41) facilitated hippocampal long-term memory
67 formation in response to a learning stimulus typically insufficient for forming long-term
68 memory. This finding was associated with increased long-term potentiation (LTP) as well
69 as modulations to synaptic physiology in hippocampal CA1[17]. Notably, the hippocampal
70 memory effects of juvenile ELE during P21-27 persisted two weeks after exercise
71 cessation, which is longer than the effect of exercise on adult hippocampal function[23].
72 Taking the early-life and adult exercise findings together, it is possible that exercise may
73 "prime" hippocampal function for response to future experiences. The epigenome is a
74 strong consideration for this priming effect of exercise: it could serve as a platform for
75 the molecular memory of exercise by promoting efficient gene expression and
76 modulating behavioral output[28]. The mechanisms underlying sustained
77 electrophysiological and behavioral effects of ELE have not been assessed from the
78 perspective of a potential molecular memory of ELE within the epigenome.
79 In this study we describe a new approach to simultaneously isolate neuron-
80 specific chromatin and translating mRNA from a single hippocampal homogenate. Using
81 this approach, we discover epigenetic signatures of ELE that promote enhancements to
82 memory and plasticity in the developing brain. We identify unique neuronal gene
83 expression programs as a resulting from ELE and pair this data with ELE-induced
84 changes in H4K8ac or H3K27me3. By crossing an Emx1- Cre transgenic line with mice
85 harboring the NuTRAP (Nuclear tagging and Translating Ribosome Affinity
86 Purification[29]) cassette (termed "Emx1-NuTRAP" mice) we isolate whole nuclei and
87 translating mRNA from a single hippocampus by combining the first steps of the
88 INTACT (Isolation of Nuclei TAgged in specific Cell Types[30]) and TRAP (Translating
89 Ribosome Affinity Purification[31]) protocols. We have named this protocol "SIT"
90 (Simultaneous INTACT & TRAP). This approach yields DNA and RNA from the same
91 homogenate that is of high-quality and sufficient concentrations for our downstream
92 sequencing procedures RNA- and CUT&RUN-seq. Using previously undescribed
93 technical approaches for neuron-specific, paired transcriptomic and epigenomic bulk

94 sequencing, this study uncovers hippocampal gene expression programs and associated
95 histone modifications that are driven by ELE to promote plasticity. Importantly, these
96 data reveal an epigenetic signature resulting from ELE that may form the basis of
97 persistently enabled hippocampal function.
98

99 **Results**

100 **"Emx1-NuTRAP" mouse allows for simultaneous isolation of nuclear chromatin**
101 **and translating mRNA from a single population of hippocampal neurons.**

102 Our initial goal was to obtain translating mRNA and nuclear DNA from a single
103 population of neurons to couple transcriptional network changes with alterations in
104 histone modifications resulting from ELE. To do this, we developed a new transgenic
105 mouse line (Emx1-NuTRAP) and experimental protocol (SIT protocol). We crossed male
106 NuTRAP reporter mice[29] with female Emx1-Cre[32,33] mouse lines to generate Emx1-Cre;
107 NuTRAP transgenic progeny for this study (Fig. 1A). Emx1-expressing neurons are
108 predominately excitatory[32] and are necessary for hippocampal neurogenesis and motor
109 skill learning[34]. In the presence of a *loxP* site-flanked sequence, Emx1-Cre facilitates
110 recombination in approximately 88% of neurons in the neocortex and hippocampus, and
111 in less than 2% of GABAergic inhibitory interneurons in these regions[32]. Emx1-Cre also
112 targets neural progenitor cells and can be expressed in mature astrocytes in striatum[35]. Of
113 note, we exclusively used Emx1-Cre female mice in our breeding schemes given that the
114 Cre-recombinase has been reported to be expressed in a subset of male germline cells[36].

115 We sought to validate neuron-specific expression of the NuTRAP cassette. First,
116 immunohistochemistry of Emx1-NuTRAP hippocampal slices show distinct GFP and
117 mCherry expression in CA1 and CA3 pyramidal neurons (Fig. 1B-C) as well as the
118 granule cell layer of the dentate gyrus (DG; Fig. 1D). Furthermore, mCherry positive
119 nuclei remained intact and bound to the magnetic beads after our modified nuclear
120 isolation procedure (Supplementary Fig. 1A). As Emx1-expressing neural stem cells can
121 become astrocytes[32], we sought to determine whether a significant number of mature
122 astrocytes were obtained in the population of isolated cells. Flow cytometry experiments
123 using THY-1 as a neuronal marker and S100β as an astrocytic marker revealed a distinct
124 population of cells double positive for GFP and THY-1, whereas a S100β and GFP
125 double positive cell population was absent (Fig. 1E and Supplementary Table 1).

126 To perform SIT, hippocampal tissue was dissected from both brain hemispheres,
127 combined, and homogenized in one sample tube (Fig. 1A). We then performed the
128 INTACT and TRAP methods on isolated samples by starting the protocol with the
129 beginning steps from the INTACT procedure, modified to include cycloheximide.

130 Cycloheximide works rapidly to inhibit protein synthesis and is used for maintaining
131 crosslinks between translating mRNA and ribosomal subunits during purification in the
132 traditional TRAP method. Despite the presence of cycloheximide, nuclear morphology
133 from Emx1-expressing neurons is overall unchanged (Supplementary Fig. 1A).
134 Additionally, a Bioanalyzer was used to determine if there were cycloheximide-induced
135 double-stranded DNA breaks in our nuclear preparation that could interfere with
136 downstream DNA sequencing applications (such as ATAC, CUT&RUN, or CUT&Tag).
137 We found no evidence of DNA double strand breaks generating fragments of less than
138 1kb (Supplementary Fig. 2A). Following magnetic purification of biotin-labeled nuclei,
139 the supernatant fraction was removed and taken through TRAP, while the pelleted nuclei
140 were processed through the remaining steps of INTACT (see Methods). Using qPCR, we
141 found that TRAP isolated mRNA had significantly reduced expression of *Mog* and
142 *Cd11b* compared to total RNA, suggesting depletion of oligodendrocyte and microglial
143 populations in TRAP mRNA (Supplementary Fig. 1B). Combining bilateral hippocampi
144 from a single mouse yielded TRAP-isolated mRNA of high quality and sufficient
145 concentration for sequencing (RIN > 8 for all samples, average yield RNA = 14.36688
146 ng/ul; Supplementary Table 2 and Supplementary Fig. 2B). INTACT-isolated nuclei were
147 further processed using the CUT&RUN (Cleavage Under Targets and Release Using
148 Nuclease[37]) method to isolate antibody-specific protein-DNA interactions for
149 downstream DNA sequencing. The resulting DNA libraries were of high quality and
150 concentration when using specific antibodies (H4K8ac: average size = 1197 bp, average
151 concentration = 127.8 nM; H3K27me3: average size = 1056 bp, average concentration =
152 139.0 nM; Supplementary Table 2). In contrast, the resulting DNA libraries using the
153 non-specific IgG control had substantially lower concentrations (IgG: average size =
154 1075 bp, average concentration = 16.3 nM; Supplementary Table 2) further indicating
155 that nuclear DNA from both isolations was of high starting quality.
156 To confirm our TRAP-isolated hippocampal mRNA came primarily from
157 excitatory neurons, we took a bioinformatics approach to assess for neuronal gene
158 enrichment. Specifically, we compared RNA-seq data from whole dorsal hippocampal
159 tissue of wild-type mice to our TRAP-isolated RNA-seq data. We found that TRAP-
160 isolated mRNA had significant enrichment of several neuronal genes including *Dlg4*,

161 *Thy1*, *Eno2*, and *Syt4*, as well as a significant reduction in astrocytic, microglial,
162 oligodendrocyte, and inhibitory neuron genes (Fig. 1F). There was a relative expression
163 increase of the glial fibrillary astrocytic protein (GFAP) in our TRAP samples. This gene
164 can also be expressed in neural stem populations that were present in our whole
165 hippocampus samples, so this finding may be a reflection of the neural stem cell
166 population of the dentate gyrus captured as part of our TRAP isolation[38,39]. Overall, these
167 findings suggest that the Emx1-NuTRAP mouse model is a valid tool for neuron-enriched
168 isolation of sequencing-grade, translating mRNA and nuclear chromatin from the same
169 cell homogenate.

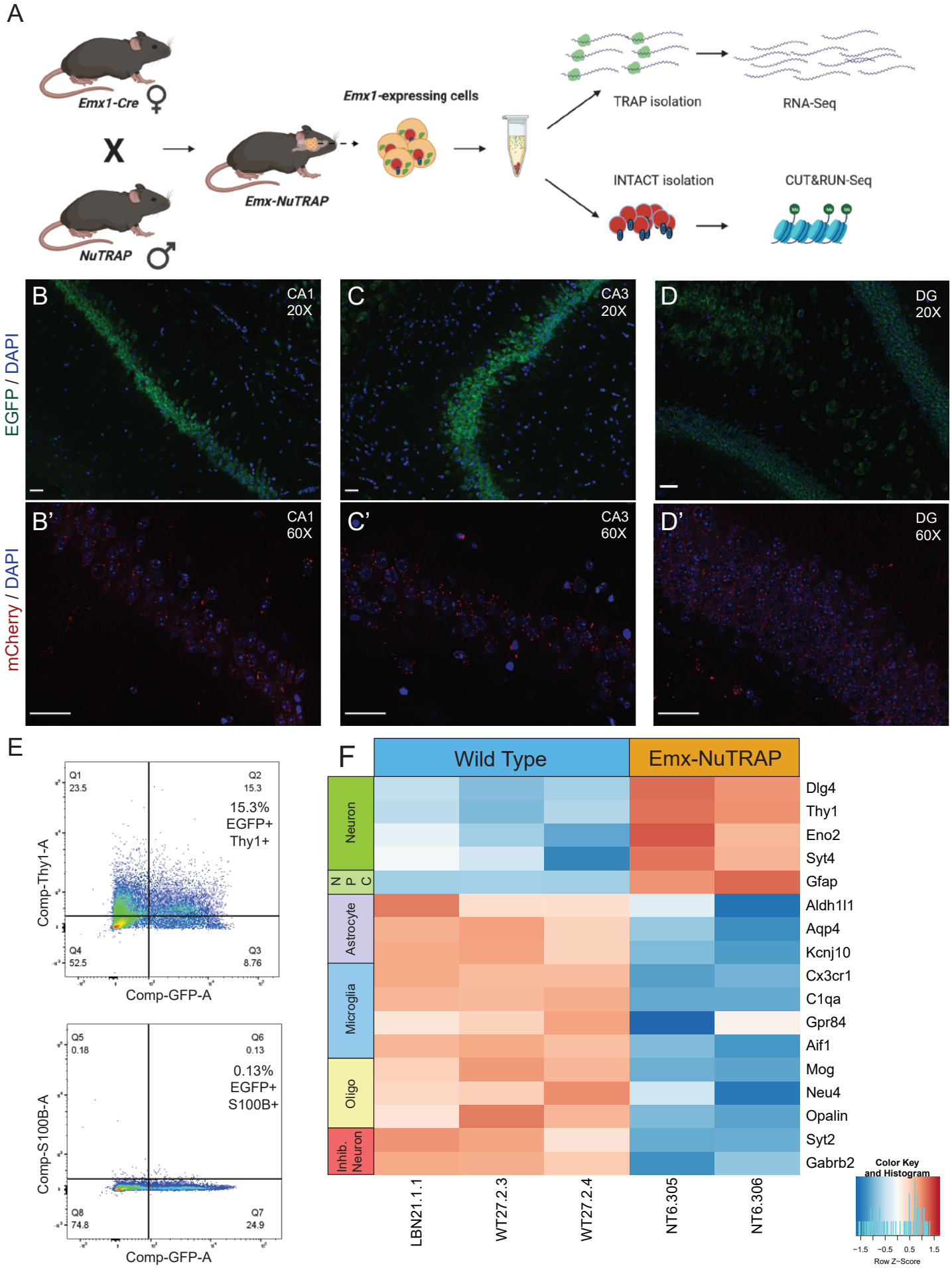
A
Emx1-Cre
X
NuTRAP
Emx-NuTRAP
Emx1-expressing cells
TRAP isolation
RNA-Seq
INTACT isolation
CUT&RUN-Seq
B
CA1
20X
C
CA3
20X
D
DG
20X
B'
CA1
60X
C'
CA3
60X
D'
DG
60X
EGFP / DAPI
mCherry / DAPI
E
Q1
23.5
Q2
15.3
15.3%
EGFP+
Thy1+
Q4
52.5
Q3
8.76
Comp-Thy1-A
Comp-GFP-A
Q5
0.18
Q6
0.13
0.13%
EGFP+
S100B+
Q8
74.8
Q7
24.9
Comp-S100B-A
Comp-GFP-A
F
Wild Type
Emx-NuTRAP
Neuron
N
P
C
Astrocyte
Microglia
Oligo
Inhib. Neuron
Dlg4
Thy1
Eno2
Syt4
Gfap
Aldh1l1
Aqp4
Kcnj10
Cx3cr1
C1qa
Gpr84
Aif1
Mog
Neu4
Opalin
Syt2
Gabrb2
LBN21.1.1
WT27.2.3
WT27.2.4
NT6.305
NT6.306
Color Key and Histogram
−1.5
−0.5
0.5
1.5
Row Z−Score

170 **Figure 1. Generation and validation of the Emx1-NuTRAP mouse** (A) Schematic
171 representation of the Emx1-NuTRAP mouse generation and workflow of the SIT
172 protocol. (B) Immunofluorescence imaging of the CA1 region of the hippocampus at 20x
173 objective and (B') 60x objective after incubation with an mCherry antibody overnight.
174 (C) Immunofluorescence imaging of the CA3 and CA2 region of the hippocampus at 20x
175 objective and (C') 60x objective after incubation with an mCherry antibody overnight.
176 (D) Immunofluorescence imaging of the DG region of the hippocampus at 20x objective
177 and (D') 60x objective after incubation with an mCherry antibody overnight. Scale bars
178 are set to 50µm for all images (B-D). (E) Flow cytometry for EGFP, THY-1, and S100β
179 (15.3% of cells THY-1+/EGFP+ and 0.13% of cells S100β+/EGFP+). (F) Heatmap of
180 differentially expressed neuronal and other cell type markers from RNA-seq data
181 comparing TRAP isolated RNA from our Emx1-NuTRAP mice and previously generated
182 dorsal hippocampal tissue RNA from wild type.

183 **Performing INTACT/TRAP on the same or separate cell suspensions yields highly**
184 **comparable RNA-seq and CUT&RUN-seq results.**
185 Previous methods for performing INTACT and TRAP using NuTRAP mice have
186 taken separate tissue homogenates for each procedure[29,40]. In this study, we performed
187 SIT on a single tissue homogenate containing bilateral hippocampi (the products of SIT
188 are referred to as "simultaneous isolations"). To determine if our approach of SIT
189 compares well with separate INTACT and TRAP procedures, we also performed separate
190 INTACT and TRAP from hippocampal tissue obtained from one brain hemisphere for
191 each method, counterbalancing for left versus right hemispheres (we refer to this protocol
192 as "separate isolations"). A Bioanalyzer was used to determine the amount and quality of
193 the RNA obtained from each type of isolation (Separate isolations: average RNA
194 concentration = 7.805 ng/ul, average RIN = 9.5; Simultaneous isolations: average RNA
195 concentration = 14.367 ng/ul, average RIN = 9.3; Supplementary Table 2). The average
196 RNA yield from the separate isolations (using a unilateral hippocampus) was
197 approximately equal to half of the average yield of the simultaneous isolations (which
198 combined bilateral hippocampi; Supplementary Table 2). Similarly, the final library
199 concentrations for the separately isolated IgG CUT&RUN-seq libraries were also
200 approximately half the concentration of the simultaneous isolations (average
201 simultaneous: 24.2nM, average separate: 11nM; Supplementary Table 2). We interpret
202 this to mean that nuclear DNA was fully intact in the simultaneous isolation because we
203 did not obtain substantially more than double the concentration in the simultaneous vs
204 separate isolations. Unilateral hippocampal homogenates yielded sufficient sequencing
205 concentrations and quality to allow for library preparations from individual mice
206 (Supplementary Table 2).
207 To determine if normalized RNA-seq counts were similar between the two isolation
208 methods, we performed a Spearman's correlation between the datasets from sedentary
209 mice. The two RNA-seq datasets were found to be highly correlated, with R values
210 greater than 0.5 and p value less than 2.2×10^{-16} ($R=1$, $p<2.2\times10^{-16}$; Fig. 2A).
211 CUT&RUN-seq was used to identify genomic regions interacting with either H4K8ac, an
212 activating histone post-translational modification (PTM), or H3K27me3, a generally
213 repressive histone PTM. We again applied Spearman's correlation to understand whether

214 the simultaneous vs separate INTACT isolation methods could influence CUT&RUN-seq
215 peak distribution. We compared normalized count data for CUT&RUN-seq peaks across
216 a representative chromosome (chromosome 2). We binned 100bp increments along the
217 entire chromosome from the simultaneous and separate isolations using datasets
218 generated from sedentary mice. Normalized sequencing counts, which reflected reads
219 assigned to binned genomic regions along chromosome 2, were highly similar between
220 conditions (H4K8ac: $R=0.65$, $p<2.2x10^{-16}$, H3K27me3: $R=0.81$, $p<2.2x10^{-16}$; Fig. 2B-C).
221 Taken together, these experiments suggest that translating mRNA and nuclear DNA
222 isolated from hippocampal homogenates using either simultaneous or separate isolation
223 procedures are comparable in terms of quality, concentration, functional characterization,
224 and normalized sequencing reads.
225 We next wanted to determine if the different isolation methods could bias resulting
226 gene expression on the basis of gene length. When plotting gene length against log fold
227 change of gene expression, we see a similar distribution pattern of ELE-induced
228 differentially expressed hippocampal genes (DEGs) between the simultaneous and
229 separate methods (Fig. 2D-E). We then compared the ELE-induced DEGs obtained using
230 either the separate or the simultaneous isolation methods. Although many of the genes
231 did not overlap (Fig. 2F-G and Supplementary Table 3), most Gene Ontology (GO) terms
232 did (14/20 GO terms for upregulated genes and 15/17 for downregulated genes; Fig. 2H-
233 K and Supplementary Table 3).

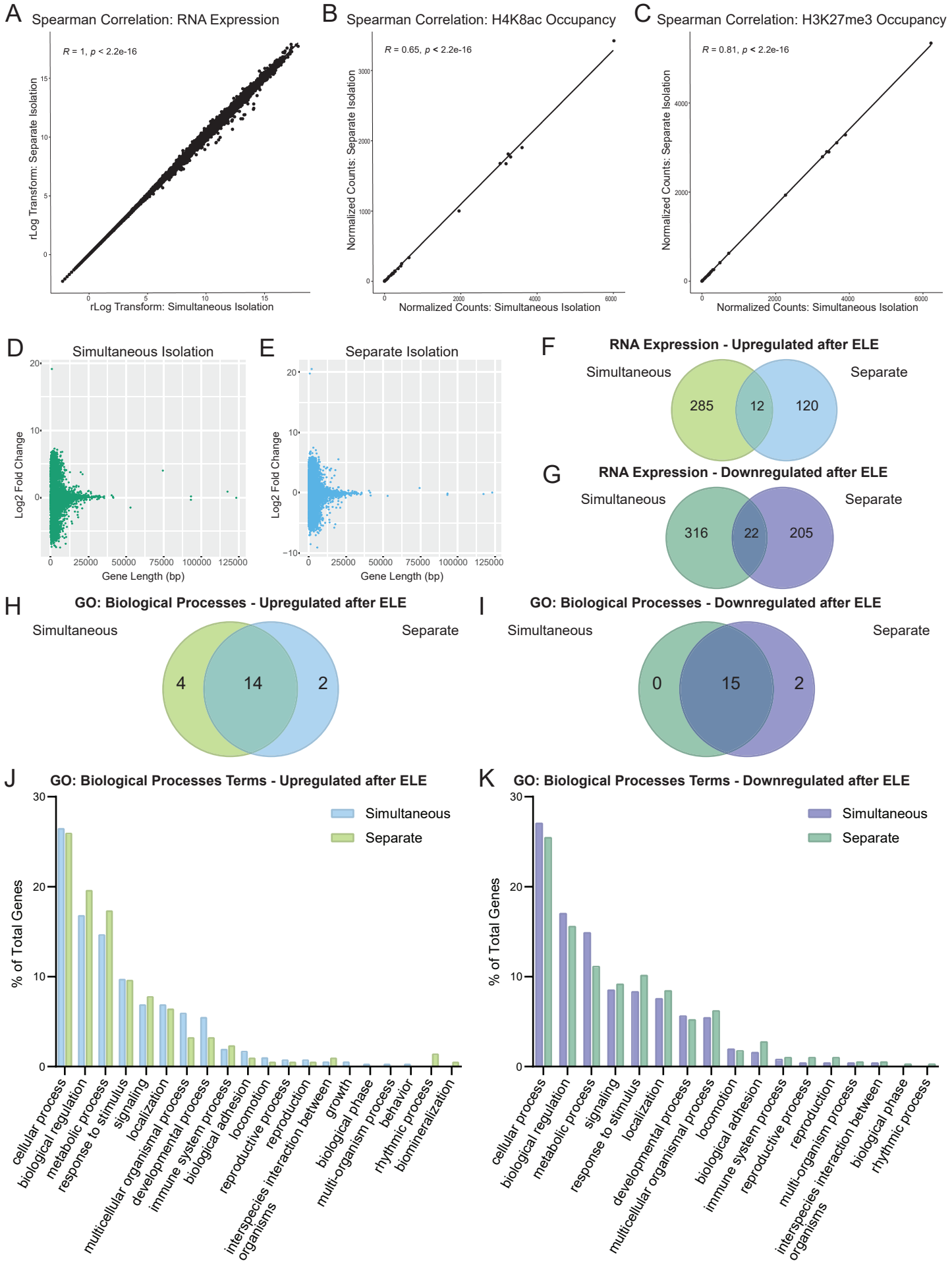
A
Spearman Correlation: RNA Expression
R = 1, p < 2.2e-16
rLog Transform: Separate Isolation
rLog Transform: Simultaneous Isolation
B
Spearman Correlation: H4K8ac Occupancy
R = 0.65, p < 2.2e-16
Normalized Counts: Separate Isolation
Normalized Counts: Simultaneous Isolation
C
Spearman Correlation: H3K27me3 Occupancy
R = 0.81, p < 2.2e-16
Normalized Counts: Separate Isolation
Normalized Counts: Simultaneous Isolation
D
Simultaneous Isolation
Log2 Fold Change
Gene Length (bp)
E
Separate Isolation
Log2 Fold Change
Gene Length (bp)
F
RNA Expression - Upregulated after ELE
Simultaneous
Separate
285
12
120
G
RNA Expression - Downregulated after ELE
Simultaneous
Separate
316
22
205
H
GO: Biological Processes - Upregulated after ELE
Simultaneous
Separate
4
14
2
I
GO: Biological Processes - Downregulated after ELE
Simultaneous
Separate
0
15
2
J
GO: Biological Processes Terms - Upregulated after ELE
Simultaneous
Separate
% of Total Genes
cellular process
biological regulation
metabolic process
response to stimulus
signaling
localization
multicellular organismal process
developmental process
immune system process
biological adhesion
locomotion
reproductive process
reproduction
interspecies interaction between organisms
growth
biological phase
multi-organism process
behavior
rhythmic process
biomineralization
K
GO: Biological Processes Terms - Downregulated after ELE
Simultaneous
Separate
% of Total Genes
cellular process
biological regulation
metabolic process
signaling
response to stimulus
localization
developmental process
multicellular organismal process
locomotion
biological adhesion
immune system process
reproductive process
reproduction
multi-organism process
interspecies interaction between organisms
biological phase
rhythmic process

234 **Figure 2. Simultaneous and separate isolations of DNA and RNA from Emx1-**
235 **NuTRAP mice are comparable.** For Fig. 2A-E, n=2 mice for simultaneous isolations
236 and n=3 mice for separate isolations. (A) Spearman's correlation for RNA expression
237 between separately isolated RNA and simultaneously isolated RNA (R=1, $p<2.2x10^{-16}$).
238 (B) Spearman's correlation between separate and simultaneously isolated DNA from
239 CUT&RUN-seq for H4K8ac with 100bp chromosome 2 position bins (R=0.65, $p<2.2x10^{-}$
240 ^{16}). (C) Spearman's correlation between separate and simultaneously isolated DNA from
241 CUT&RUN-seq for H3K27me3 with 100bp chromosome 2 position bins (R=0.81,
242 $p<2.2x10^{-16}$). (D) Gene length versus fold change distribution plot for simultaneously
243 isolated RNA. (E) Gene length versus fold change distribution plot for separately isolated
244 RNA. (F) Genes upregulated in Emx1-NuTRAP RNA-seq after ELE in either
245 simultaneous (n=2 sedentary mice and n=3 ELE mice) or separate isolations (n=3 mice
246 per group). (G) Genes downregulated in Emx1-NuTRAP RNA-seq after ELE in either
247 simultaneous or separate isolations. (H, I) Panther Gene Ontology: Biological Processes
248 Venn diagram (H) and bar graph of gene distributions (I) for genes upregulated after ELE
249 in either separate or simultaneous isolations. (J, K) Panther Gene Ontology: Biological
250 Processes Venn diagram (J) and bar graph of gene distributions (K) for genes
251 downregulated after ELE in either separate or simultaneous isolations.

252 **Neuron-specific gene expression and histone PTMs are functionally comparable**
253 **between left and right hippocampal hemispheres.**
254 Many studies take advantage of the brain's structural symmetry by using tissue
255 from each hemisphere for separate molecular processing. Prior evidence demonstrates
256 that hippocampal lateralization can influence LTP, hemisphere-specific glutamate
257 receptor density, and performance in certain memory tasks[41]. We wanted to determine if
258 there were differences in transcriptional programs resulting from ELE in left vs right
259 hippocampi. Using the separate isolation approach described above, we compared ELE-
260 induced differential gene expression between left and right hemispheres. We found that
261 although individual gene expression patterns were different between hippocampi
262 originating in the left and right brain hemispheres (Fig. 3A-B and Supplementary Table
263 4), the Panther GO: Biological Processes terms were substantially similar with most
264 categories overlapping (Fig. 3C-F and Supplementary Table 4). This could suggest
265 spatial or hemispheric assignment of genes with functional similarity.
266 Finally, we wanted to determine if left and right hippocampal hemispheres had
267 significant differences in DEGs and CUT&RUN-seq peak distributions at baseline
268 (without exercise). We performed Spearman's correlation on the transcript counts from
269 the RNA-seq ($R=1$, $p<2.2x10^{-16}$; Fig. 3G), and the CUT&RUN-seq 100 bp binned peak
270 counts along chromosome 2 for H3K27me3 ($R=0.70$, $p<2.2x10^{-16}$; Fig. 3H) and for
271 H4K8ac ($R=0.59$, $p<2.2x10^{-16}$; Fig. 3I). .We found that the seq peaks and transcript
272 counts were very similar with significance considered as R values greater than 0.5 and p
273 value less than 2.2×10^{-16} (Fig. 3G-I). These data suggest that in the sedentary condition,
274 left and right hippocampal hemispheres yield similar normalized sequencing counts.

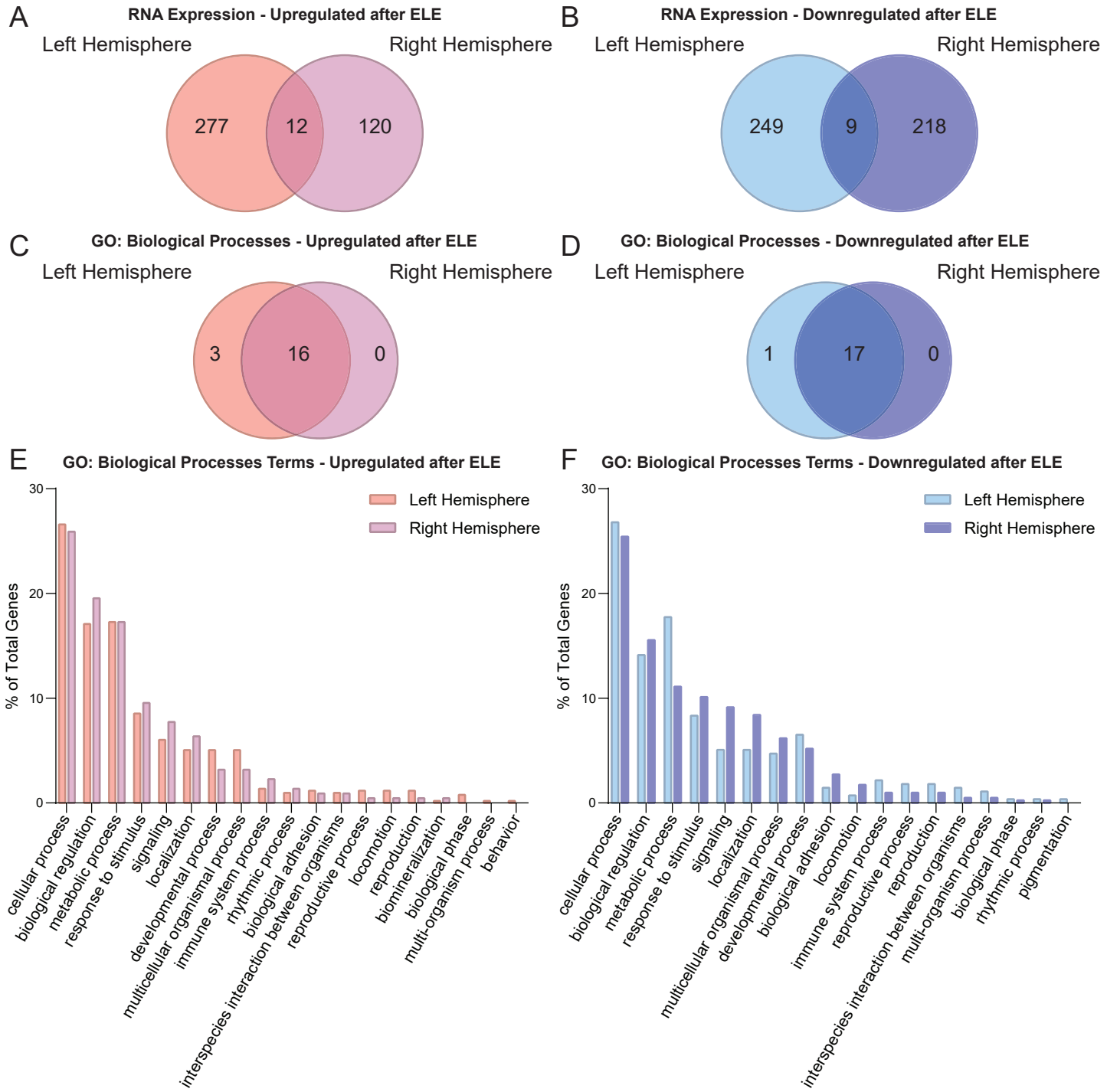
A
RNA Expression - Upregulated after ELE
Left Hemisphere
Right Hemisphere
277
12
120
B
RNA Expression - Downregulated after ELE
Left Hemisphere
Right Hemisphere
249
9
218
C
GO: Biological Processes - Upregulated after ELE
Left Hemisphere
Right Hemisphere
3
16
0
D
GO: Biological Processes - Downregulated after ELE
Left Hemisphere
Right Hemisphere
1
17
0
E
GO: Biological Processes Terms - Upregulated after ELE
Left Hemisphere
Right Hemisphere
% of Total Genes
0
10
20
30
cellular process
biological regulation
metabolic process
response to stimulus
signaling
localization
developmental process
multicellular organismal process
immune system process
rhythmic process
biological adhesion
interspecies interaction between organisms
reproductive process
locomotion
reproduction
biomineralization
biological phase
multi-organism process
behavior
F
GO: Biological Processes Terms - Downregulated after ELE
Left Hemisphere
Right Hemisphere
% of Total Genes
0
10
20
30
cellular process
biological regulation
metabolic process
response to stimulus
signaling
localization
multicellular organismal process
developmental process
biological adhesion
locomotion
immune system process
reproductive process
reproduction
interspecies interaction between organisms
multi-organism process
biological phase
rhythmic process
pigmentation
G
Spearman Correlation: RNA Expression
R = 1, p < 2.2e−16
rLog Transform: Left Hemisphere
rLog Transform: Right Hemisphere
0
5
10
15
H
Spearman Correlation: H4K8ac Occupancy
R = 0.59, p < 2.2e-16
Normalized Counts: Left Hemisphere
Normalized Counts: Right Hemisphere
0
1000
2000
3000
I
Spearman Correlation: H3K27me3 Occupancy
R = 0.7, p < 2.2e-16
Normalized Counts: Left Hemisphere
Normalized Counts: Right Hemisphere
0
2000
4000

275 **Figure 3: Histone modifications and functional categorizations of gene expression**
276 **are similar regardless of hemispheric origin of hippocampal tissue.** (A-B) Venn
277 diagram of genes upregulated (A) or downregulated (B) by ELE identified between the
278 left and right hemispheres by the separate isolation protocol RNA-seq (n=3 mice per
279 group). (C-D) Venn diagram of Panther Gene Ontology: Biological Process terms for
280 genes upregulated (C) or downregulated (D) by ELE identified between the left and right
281 hemispheres by the separate isolation protocol RNA-seq. (E-F) Percent of genes fitting
282 into each GO category for the left and right hemisphere for genes upregulated (E) and
283 downregulated (F) by ELE by separate isolation RNA-seq. (G) Spearman's correlation
284 between the left and right hemispheres RNA-seq data from the separate isolation protocol
285 of sedentary rlog normalized expression ($R=1$, $p<2.2x10^{-16}$). (H) Spearman's correlation
286 between hemispheres for CUT&RUN-seq for H4K8ac normalized count data for
287 chromosome 2 in 100bp bins ($R=0.59$, $p<2.2x10^{-16}$). (I) Spearman's correlation between
288 hemispheres for CUT&RUN-seq for H3K27me3 normalized count data for chromosome
289 2 in 100bp bins ($R=0.7$, $p<2.2x10^{-16}$).

290 **Early-life exercise promotes expression of plasticity-related genes and is associated**
291 **with transcriptional regulatory pathways implicated in hippocampal memory.**
292 To identify the transcriptional effects of ELE in hippocampal neurons, we performed
293 cell-type specific bulk sequencing on RNA extracted from Emx1-NuTRAP hippocampi
294 using the SIT approach. We compared DEGs from sedentary mice vs mice that
295 underwent voluntary wheel running between postnatal days (P) 21-41 (Supplementary
296 Fig. 1C). Using DESeq2 to assess for DEGs (>30% expression increase with a p value <
297 0.05), we found that voluntary exercise during juvenile-adolescence significantly alters
298 gene expression in Emx1 expressing neurons (297 upregulated and 338 downregulated
299 genes; Fig. 4A and Supplementary Table 3). Many of the genes upregulated after ELE are
300 also known to be involved in exercise or hippocampal memory mechanisms, including
301 *Bdnf*[42] and *Nr4a1*[43]. To functionally categorize ELE-induced DEGs, we performed a
302 Panther Gene Ontology (GO) analysis[44] focusing on the Molecular Function
303 categorization and separated by upregulated and downregulated genes. The GO term
304 categories with the most genes functionally assigned to them were binding, catalytic
305 activity, molecular function regulator, transporter activity, molecular transducer activity,
306 and structural molecule activity (Fig. 4B). Many of the genes driving these results are
307 known to be important in neuronal function (*Kcna1, Slc24a4, Stxbp5l, Gabra2,* and
308 *Camk2n2*), neurodevelopment (*Artn, Kdm7a, Sox21, Gap43,* and *Efna5*), and
309 hippocampal memory (*Bdnf, Nr4a1* and *Dusp5*).
310 To evaluate possible transcription factors and upstream regulators implicated by ELE-
311 induced DEGs, we applied Qiagen's Ingenuity Pathway Analysis (IPA) to our RNA-seq
312 dataset[45]. We identified significant canonical signaling pathways implicated in ELE
313 effects on hippocampal neuronal function (Supplementary Fig. 4A and Supplementary
314 Table 5). Additionally, the top six upstream regulators by significance included CREB1,
315 KMT2A, LEF1, SMAD3, EGR1, and MITF. Each of the top five transcription factors
316 have been implicated in hippocampal development or function (Fig. 4C and
317 Supplementary Table 5)[46-53]. The transcription factors KMT2A and LEF1 have not been
318 previously associated with the effects of exercise on hippocampal function. Interestingly,
319 CREB1 (through its associated CBP[54]) and KMT2A (through its methyltransferase
320 activity[47]) both have histone modifying properties. LEF1 has been shown to regulate

321 neural precursor proliferation in the hippocampus[48]. SMAD3 is critical for intermediate
322 progenitor cell survival and negatively regulates serum insulin after exercise[49,50]. EGR1 is
323 an immediate early gene that recruits TET1 DNA demethylase during neural activation
324 and development[51]. MITF was the sixth upstream regulator identified and is a
325 transcription factor linked to autophagy mechanisms[52]. These specific transcription
326 factors were not significantly differentially expressed in our RNA-seq dataset; however,
327 their activity may not be linked to a change in their own expression after ELE but rather
328 modulated by exercise to influence programs of gene expression.
329 To further understand whether the transcriptional profiles resulting from ELE were
330 enriched for specific *a priori* assigned molecular functions, we performed Gene Set
331 Enrichment Analysis (GSEA)[55]. We evaluated the "Reactome" category of functional
332 gene sets followed by a leading-edge analysis to further determine which genes were
333 driving the significant categories (Fig. 4D and Supplementary Table 6). Of the DEGs
334 upregulated after ELE, several interesting categorizations and the genes driving them
335 were revealed. The genes *H3c4*, *H2bc3*, *H2bc5*, and *H2bc9* genes, which encode histone
336 family member proteins, were driving the categories DNA methylation, HDACs
337 deacetylate histones, and transcriptional regulation by smRNAs. Meiosis and meiotic
338 recombination also emerged in these results which was unusual; however, leading edge
339 analysis showed many of these genes (*Atm, Blm, Msh4*, and *Mnd1*) to be generally
340 involved in cell-cycling processes. Exercise is well known to increase adult neurogenesis
341 in hippocampal dentate gyrus and can explain cell cycle gene enrichment in our dataset[16].
342 Several nucleoporin complex genes (*Nup35/ 42/ 43/ 50/ 58/ 62/ 93/ 107/ 153/ 210*) were
343 also identified for their associations with categories such as: gene silencing by RNA,
344 nuclear envelope breakdown, transport of mature mRNAs derived from intronless
345 transcripts. *Nup* genes form a variety of nuclear pore complexes that play critical roles in
346 cellular processes including cell-cycle regulation, cellular differentiation, and epigenetic
347 control[56].
348 Of the downregulated pathways identified, translation-associated categories
349 (translation, eukaryotic translation initiation/elongation, and SRP-dependent co-
350 translational protein targeting to membrane) were driven by significant downregulation of
351 ribosomal protein gene families (*Rps*, *Rpl*, *Rplp*) and eukaryotic initiation factor 3 (*eIF3*)

352 subunits. Over-expression of *eIF3* subunits has been linked to Parkinson's Disease and
353 altered expression of *eIF3* has been associated with neurodevelopmental disorders[57].
354 Additionally, collagen genes (*Col1a1*, *Col1a2*, *Col2a1*, *Col3a1*, and *Col5a1*) were
355 downregulated after ELE, leading to the identification of categories including: MET
356 activates PTK2 signaling, MET promotes cell motility, and collagen degradation. *Col1a1*
357 and *Col1a2* have been previously identified as putative aging genes that decrease in their
358 expression after chronic exercise in adults[58]. By analyzing these enriched pathways and
359 the networks of genes driving them, we were able to identify several transcriptional
360 programs activated by ELE that could be candidates for further exploration.

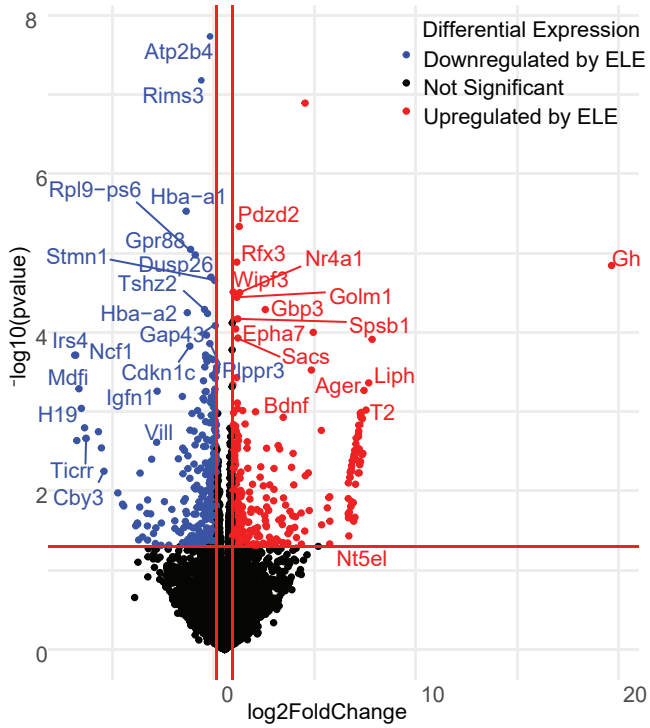

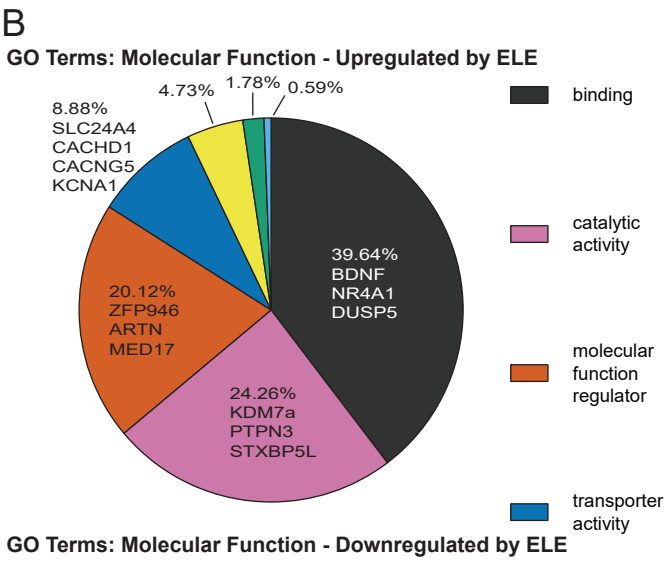

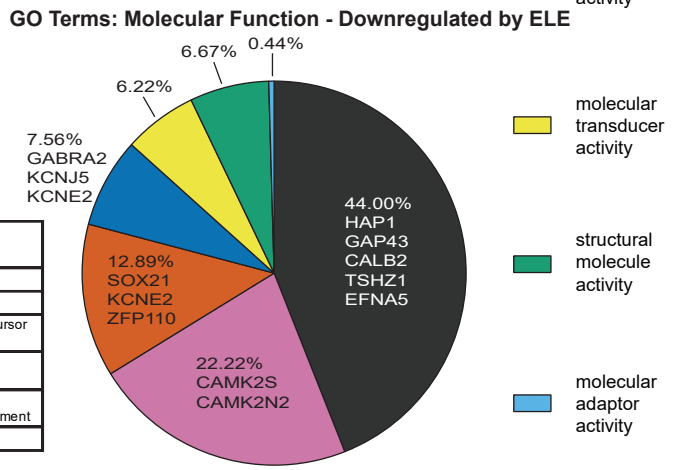

C

Predicted Activated Upstream Regulator	p-value of overlap	# Target Molecules in Dataset	Function
CREB1	1.11E-03	14	Transcription factor required for LTM
KMT2A	1.90E-03	5	Lysine methyltransferase active in development
LEF1	4.12E-03	6	Transcription factor that may regulate neural precursor cell proliferation in the hippocampus
SMAD3	1.80E-02	7	Critical for intermediate progenitor cell survival and negatively regulates serum Irisin after exercise
EGR1	3.52E-02	5	Immediate early gene that recruits TET1DNA demethylase during neural activation and development
MITF	3.58E-02	6	Transcription factor import for autophagy

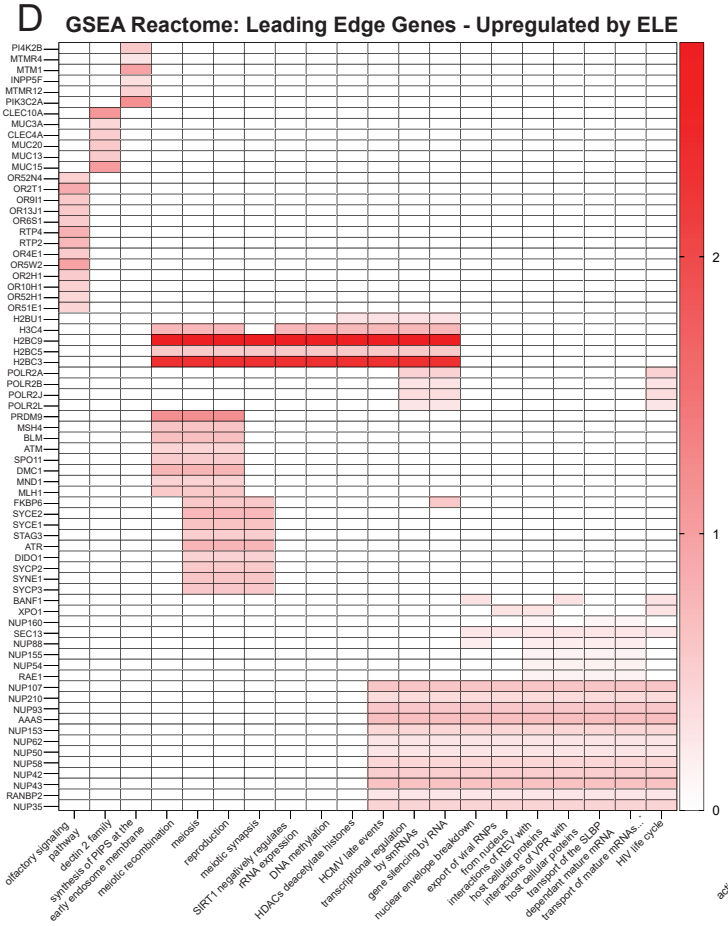

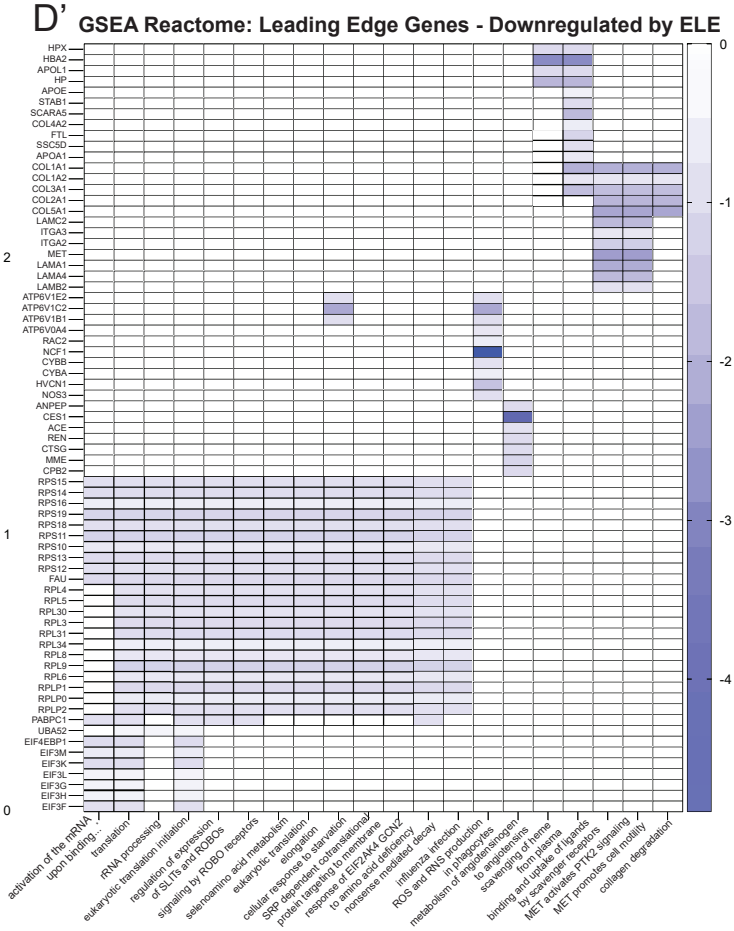

361 **Figure 4: ELE leads to transcriptomic changes in hippocampal neurons during**
362 **adolescence.** (A) Volcano plot of differentially expressed genes reaching significance
363 identified by RNA-seq on ELE versus sedentary (n=2 sedentary mice and n=3 ELE mice,
364 absolute value $\log_2$ fold change > 0.3785 and p-value < 0.05). (B) Panther Gene
365 Ontology: Molecular Function top terms by most genes assigned. (C) Top 6 upstream
366 regulators identified by Ingenuity Pathway Analysis (IPA). (D) Representative Gene Set
367 Enrichment Analysis: Reactome leading-edge diagrams showing genes upregulated (D)
368 or downregulated (D') in ELE, and their enrichment. *Abbreviated terms in (D) transport
369 of mature mRNAs derived from intronless transcripts, (D') activation of the mRNA upon
370 binding of the cap binding complex and EIFs and subsequent binding to 43S.

371 **Neuronal H4K8ac is enriched and H3K27me3 is reduced at a subset of plasticity**
372 **genes after ELE.**
373 The power of the Emx1-NuTRAP mouse model coupled with the SIT procedure
374 is the ability to directly correlate differential gene expression with candidate epigenetic
375 mechanisms in the same cell population. Hippocampal nuclei were obtained using
376 INTACT methods in our SIT procedure, followed by CUT&RUN-seq from nuclear
377 chromatin. We investigated ELE-induced changes in histone modifications H3K27me3
378 and H4K8ac across the genome. H4K8ac is a permissive histone modification that is
379 enriched at *Bdnf* after adult exercise, and its presence correlates with improved
380 hippocampal memory[22]. H3K27me3 is a repressive histone mark and a common control
381 in CUT&RUN-seq studies[37,59] and is decreased at the *Bdnf* promoter region after
382 contextual fear conditioning training[60]. Peaks were called using SEACR[61] and histone
383 modification enrichment peaks were overlapped with differentially expressed genes (Fig.
384 5A). We correlated H4K8ac and H3K27me3 peaks present with upregulated and
385 downregulated mRNA as a result of ELE. The loss of either H3K27me3 or H4K8ac did
386 not correlate with changes in mRNA expression. This may indicate that ELE-induced
387 additions of these two histone modifications, but not their removal, underlie differential
388 gene expression. 93 upregulated genes correlate with new H4K8ac peaks while 33
389 downregulated genes correlate with new H3K27me3 peaks (Fig. 5B and Supplementary
390 Table 7). However, loss of only one H4K8ac peak correlates with downregulation of
391 mRNA, and loss of only two H3K27me3 peaks correlate with upregulation of mRNA
392 (Fig. 5B and Supplementary Table 7). Unsurprisingly, many of the peaks we discovered
393 newly present because of ELE did not correlate with expression changes in many genes.
394 Notable upregulated genes with new H4K8ac after ELE are *Prox1*, *Sntb2*, and *Kptn*.
395 PROX1 is involved governing differentiation, maturation, and DG versus CA3 cell
396 identity in intermediate progenitor cells of the hippocampal DG[62], while SNTB2 is
397 involved in G protein-coupled receptor cell signaling[63]. KPTN encodes a protein involved
398 in cytoskeletal cell structure, and its mutation can cause neurodevelopmental disability
399 and seizures[64]. Interestingly, downregulated genes found to have new H3K27me3 after
400 ELE included *Col3a1*, *Efnb2*, *Epop*, and *Myoc*. COL3A1 and MYOC are structural
401 proteins involved in the extracellular matrix and the cytoskeleton respectively[65-67].

402 EFNB2 is a signaling molecule involved in cell migration and its haploinsufficiency can
403 cause neurodevelopmental disability[68-70]. EPOP is a known editor of the chromatin
404 landscape by altering H2Bub and H3K4me3 distributions[71,72]. Interestingly, many of the
405 histone modification changes that occurred following exercise appear to be in distal
406 intergenic regions for H3K27me3 and intronic regions for H4K8ac (Fig. 5C). To
407 investigate how ELE-induced changes to histone PTM distribution might alter gene
408 expression, we looked at the distribution of peaks around *Prox1* (Fig. 5D). Most apparent
409 changes in histone PTM peaks occurred in regions annotated as regulatory regions, rather
410 than the promoter region, which is concordant with our data showing that most histone
411 PTM changes happen outside of the promoter region. Taken together, these results
412 suggest that ELE promotes the new addition of H4K8ac and H3K27me3 PTMs to
413 regulate gene expression. Given that most identified peaks did not correlate with DEGs,
414 they may instead implicate regions of interest that are "primed" for facilitated gene
415 expression following future stimuli, such as learning.

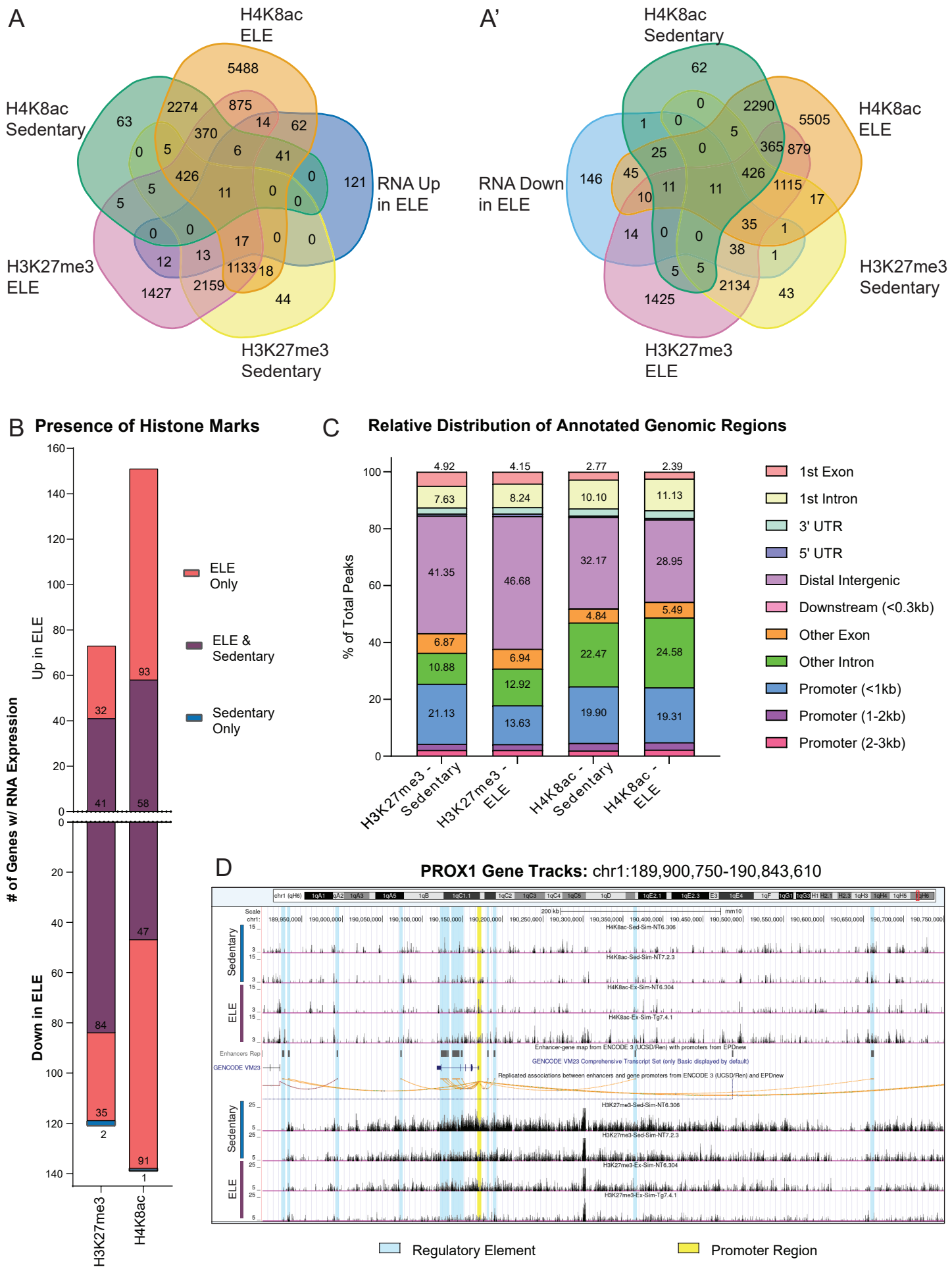
A
H4K8ac ELE
H4K8ac Sedentary
RNA Up in ELE
H3K27me3 ELE
H3K27me3 Sedentary
5488
2274
875
63
370
14
62
0
5
6
41
426
0
121
5
11
0
0
0
0
17
0
0
12
13
1133
18
1427
2159
44
A'
H4K8ac Sedentary
H4K8ac ELE
RNA Down in ELE
H3K27me3 Sedentary
H3K27me3 ELE
62
0
2290
5505
1
0
5
25
0
365
879
146
45
426
1115
10
11
11
17
35
1
14
0
0
38
1
5
5
2134
43
1425
B Presence of Histone Marks
# of Genes w/ RNA Expression
Up in ELE
Down in ELE
ELE Only
ELE & Sedentary
Sedentary Only
32
41
93
58
84
47
35
2
91
1
H3K27me3
H4K8ac
C Relative Distribution of Annotated Genomic Regions
% of Total Peaks
4.92
4.15
2.77
2.39
7.63
8.24
10.10
11.13
41.35
46.68
32.17
28.95
6.87
6.94
4.84
5.49
10.88
12.92
22.47
24.58
21.13
13.63
19.90
19.31
H3K27me3 - Sedentary
H3K27me3 - ELE
H4K8ac - Sedentary
H4K8ac - ELE
1st Exon
1st Intron
3' UTR
5' UTR
Distal Intergenic
Downstream (<0.3kb)
Other Exon
Other Intron
Promoter (<1kb)
Promoter (1-2kb)
Promoter (2-3kb)
D PROX1 Gene Tracks: chr1:189,900,750-190,843,610
Sedentary
ELE
Regulatory Element
Promoter Region

416 **Figure 5: ELE alters H4K8ac and H3K27me3 occupancy.** (A) Venn diagram of gene
417 peaks identified in CUT&RUN-seq for H4K8ac and H3K27me3 by SEACR (top 1% of
418 peaks FDR<0.1) overlapped with genes upregulated (A) and downregulated (A') in RNA
419 by ELE (n=2 sedentary mice and n=3 ELE mice). (B) CUT&RUN-seq SEACR peak calls
420 at genes that overlap with genes differentially expressed by ELE as determined by RNA-
421 seq. (C) Stacked bar of the relative distribution of peak calls at various genomic regions
422 identified by CUT&RUN-seq called using SEACR. (D) Representative track of
423 CUT&RUN-seq data around *Prox1* showing differential peak height between ELE and
424 sedentary conditions for H4K8ac and H3K27me3.

425 **ELE induces changes in H4K8ac and H3K27me3 occupancy at promoters of genes**
426 **involved in hippocampal memory consolidation.**
427 Prior work from our lab and others has found that both ELE and adult exercise
428 can facilitate hippocampal long-term memory formation in mice exposed to a typically
429 subthreshold learning event (3 minutes of object location memory (OLM) training;
430 typically insufficient for LTM formation in sedentary mice). These results suggest that
431 ELE may "prime" neuronal function to facilitate hippocampal learning. Here we test the
432 hypothesis that ELE enables memory consolidation via altering presence of the histone
433 modifications H4K8ac and H3K27me3 in promoters of genes associated with learning
434 and hippocampal plasticity. These changes could potentially allow for more rapid
435 transcription of memory-related genes. Wildtype animals underwent ELE followed by
436 object location memory training on p41 and were sacrificed 60 minutes later (during
437 memory consolidation; Fig. 6A). Dorsal hippocampi were dissected and processed for
438 RNA-seq, and these data were compared to the previously identified differential gene
439 expression, H4K8ac, and H3K27me3 occupancy after ELE without learning (generated
440 from Emx1-NuTRAP CUT&RUN-seq; Fig. 5). We categorized differentially expressed
441 genes based on the experimental group: ELE alone, ELE+3 min learning stimulus,
442 Sedentary+3 min learning stimulus, and Sedentary+10 min learning stimulus. To
443 discover ELE-induced genes "primed" for regulation during memory consolidation, we
444 focused specifically on candidate genes associated with memory after exercise (cGAME),
445 candidate genes associated with memory after exercise or sedentary (cGAMES), and
446 candidate genes associate with memory after sedentary (cGAMS) conditions (Fig. 6B,C).
447 We then evaluated cGAME and cGAMES groups of genes for the new presence or
448 absence of histone modifications H4K8ac and H3K27me3 after ELE, suggesting addition
449 or removal of these histone marks denoting a permissive (increased gene expression) or
450 repressive (reduced gene expression) chromatin state, respectively (Fig. 6B',C').
451 In the cGAMES group, there were 145 genes found to be significantly increased
452 in the mice that underwent a threshold learning event (3 min for ELE; 10 min for
453 sedentary mice). Of these 145 genes, 40% of them (58) had new H4K8ac following ELE.
454 We consider this group of genes to potentially be "primed," or readied, by ELE for rapid
455 transcription to support hippocampal memory consolidation at 3 min OLM training,

456 while also being involved in memory consolidation mechanisms in the threshold learning
457 of sedentary mice (10 min OLM training). The cGAME group of genes are those which
458 significantly increased in the ELE mice that underwent a threshold learning event but
459 were not increased in any of the other groups (including the sedentary, threshold learning
460 event / cGAMS group). These genes may be of unique importance for memory
461 consolidation specifically occurring after ELE given their absence in sedentary learners.
462 We found that the cGAME group had significant upregulation of 256 genes, with
463 approximately 30% (76) of those genes receiving new H4K8ac following ELE alone
464 (Fig. 6 B-C'). We also evaluated the cGAMES and cGAME that were significantly
465 downregulated during memory consolidation. We found 304 cGAMES and 361 cGAME
466 genes (Fig. 6 B,C). In both of these groups, a small minority of down-regulated genes had
467 altered H3K27me3 after ELE, and this was mostly gain of H3K27me3 (cGAMES: 6.3%;
468 cGAME: 6.4%) (Fig. 6 B',C'). The consolidation expression data is listed in in
469 Supplementary Table 8. The lists of overlap between these groups is listed in
470 Supplementary Table 9.
471 We wanted to determine how ELE "priming" directed gene expression during
472 memory consolidation that occurs after exercise (ELE 3min OLM) relative to sedentary
473 memory consolidation (Sed 10min OLM). We compared these to a sub-theshold learning
474 event (Sed 3min OLM training). We compared the relative $\log_2$ fold changes (LFCs) of
475 the genes in cGAME and cGAMES using z-scores for each group across the genes (Fig.
476 6D). In the vast majority of these primed genes, the ELE drove gene expression during 3
477 min of OLM in the same direction as 10 minutes of OLM training in sedentary animals
478 (Fig. 6D). In some cases the gene expression changes were more exaggerated in the same
479 direction as a sedentary threshold event (Fig. 6D). We interpret this to indicate that ELE
480 enables a 3min consolidation event to be threshold (when 10 minutes is required for a
481 sedentary mouse) by priming these genes for altered gene expression in the same
482 direction as a sedentary threshold event.
483 We next identified upstream regulators of cGAME and cGAMES genes with
484 ELE-induced histone modifications, as these mediators are likely involved in long-term
485 memory formation of a subthreshold learning event following ELE. The cGAMES and
486 cGAME lists were evaluated using Ingenuity Pathway Analysis (IPA). First, candidate

487 regulators were identified for the cGAME and cGAMES groups that have histone PTM
488 changes as a result of ELE that we measured (Fig. 6E, Supplementary Table 10).
489 Inhibition of MECP2 may indicate a reduction in DNA methylation. CREB1 is required
490 for LTM[46,73]. SNCA may play a role in neuroplasticity by modulating synaptic vesicle
491 transport[74]. Next, we wanted to identify gene networks that might be at play that are not
492 just regulated by the histone PTMs we selected. Many more histone modifications exist
493 and may regulate gene expression during consolidation in addition to those we selected.
494 We investigated the genes in cGAME and cGAMES using IPA and identified a set of
495 likely upstream regulators for these genes taken together (Fig. 6E'', Supplementary Table
496 10). Once again MECP2 inhibition and CREB1 activation appear to be indicated
497 validating their presence in the previous IPA. Notably new to this group are inhibition of
498 FMR1, KMT2D, and TCF20, along with activation of FASN, CTNNB1, and MKNK1.
499 FMR1 is involved in mRNA trafficking in neurons; so altered mRNA trafficking may be
500 an important modulator of ELE enabled consolidation. CTNNB1 is necessary for Wnt
501 signaling. Next, we interrogated what networks might be unique to exercise enabled
502 consolidation by running the cGAME list through IPA analysis (Fig. 6E', Supplementary
503 Table 10). Unique to this group, RTN4, an inhibitor of neurite outgrowth[75], was predicted
504 to trend towards inhibition. GRIN3A, a glutamatergic NMDA receptor important to
505 synaptic development and refinement[76], was predicted activated in this group. These
506 findings suggest that ELE may enable consolidation by increasing neurite and synapse
507 growth and development. TCF7L2 is also predicted to be activated. Given that this
508 transcription factor is involved in Wnt signaling, and neurogenesis[77], and activated
509 CTNNB1 is also predicted to be associated with threshold consolidation generally,
510 altered Wnt signaling may be critical for ELE enabled consolidation.

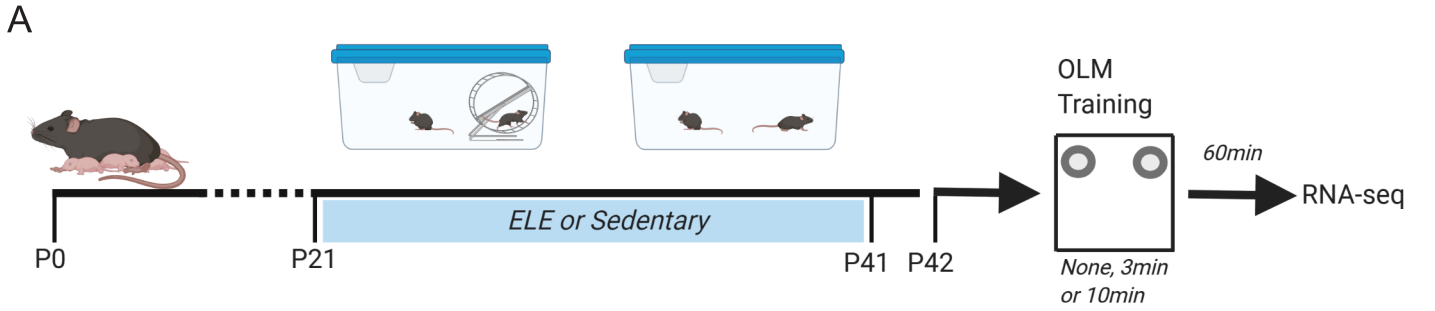

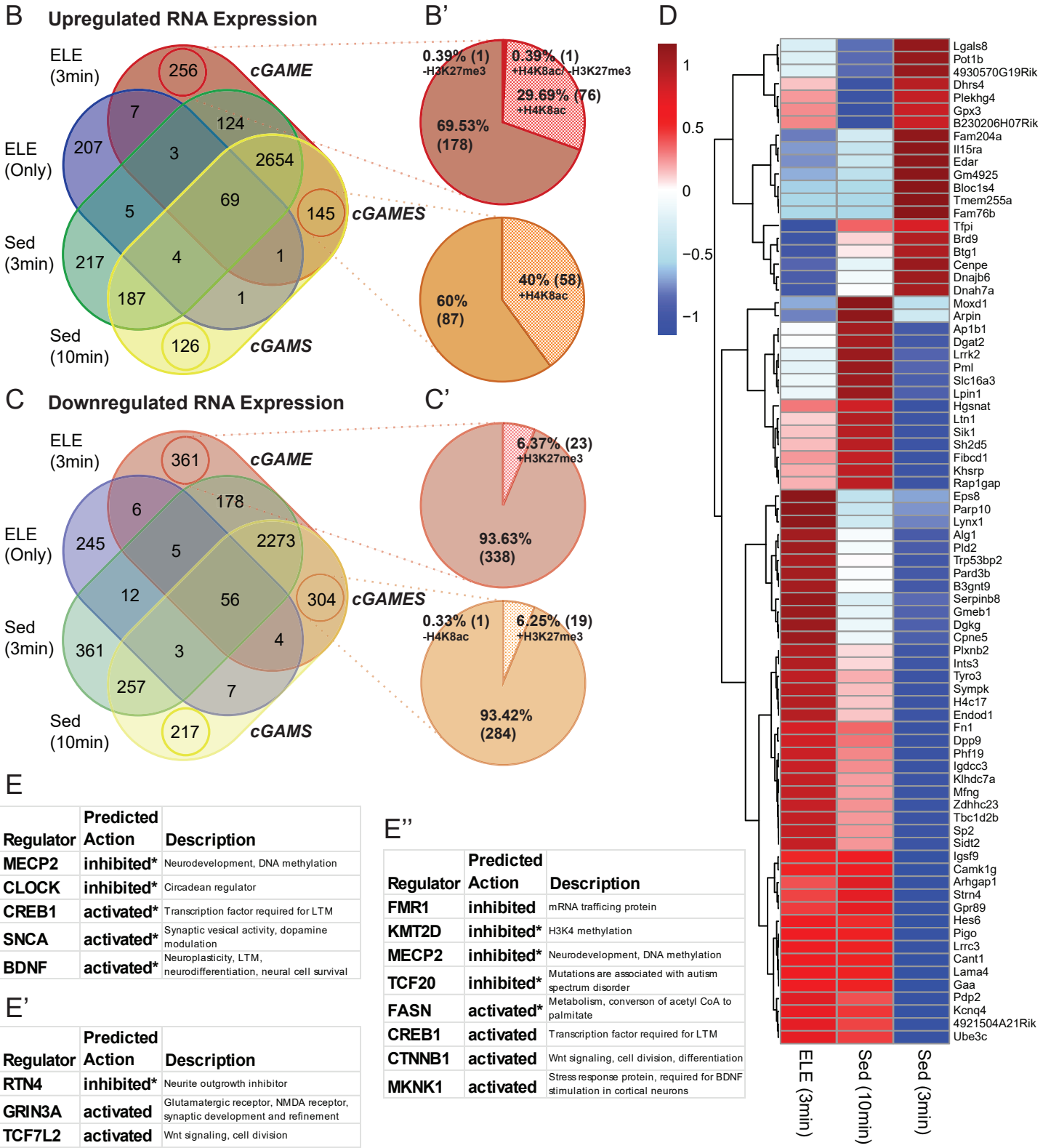

E

Regulator	Predicted Action	Description
MECP2	inhibited*	Neurodevelopment, DNA methylation
CLOCK	inhibited*	Circadean regulator
CREB1	activated*	Transcription factor required for LTM
SNCA	activated*	Synaptic vesical activity, dopamine modulation
BDNF	activated*	Neuroplasticity, LTM, neurodifferentiation, neural cell survival

E'

Regulator	Predicted Action	Description
RTN4	inhibited*	Neurite outgrowth inhibitor
GRIN3A	activated	Glutamatergic receptor, NMDA receptor, synaptic development and refinement
TCF7L2	activated	Wnt signaling, cell division

E''

Regulator	Predicted Action	Description
FMR1	inhibited	mRNA trafficing protein
KMT2D	inhibited*	H3K4 methylation
MECP2	inhibited*	Neurodevelopment, DNA methylation
TCF20	inhibited*	Mutations are associated with autism spectrum disorder
FASN	activated*	Metabolism, converson of acetyl CoA to palmitate
CREB1	activated	Transcription factor required for LTM
CTNNB1	activated	Wnt signaling, cell division, differentiation
MKNK1	activated	Stress response protein, required for BDNF stimulation in cortical neurons

511 **Figure 6: ELE may prime consolidation induced gene expression.** (A) Experimental
512 design diagram. (B) Venn diagram representing upregulated genes relative to mice
513 without ELE or learning in either ELE, ELE and 3 min OLM training, Sed and 3 min
514 OLM training, and Sed and 10 min OLM training. (B') Pie chart showing the relative
515 percentage of genes that have new H4K8ac presence or H3K27me3 loss as a result of
516 ELE in specific groups identified in the Fig. 6B labeled cGAME, and cGAMES. (C) As
517 Fig. 6B but for downregulated genes relative to mice without ELE. (C') Pie chart of
518 downregulated genes in the cGAME or cGAMES groups that have new H3K27me3 or
519 new loss of H4K8ac as a result of ELE. (D) Z-score based heatmap of genes in the
520 cGAMES and cGAME groups that have new H4K8ac or H3K27me3 presence or loss as
521 a result of ELE. Expression values used to calculate the Z-scores were relative to mice
522 that did not experience OLM training or ELE. (E) Upstream regulators identified by IPA
523 of the genes represented by Fig. 6D. (E') Upstream regulators identified by IPA of the
524 genes in the cGAME (up and downregulated) group that are unique to that when only
525 those are included in the IPA analysis (E'') Upstream regulators identified by IPA of the
526 genes in the cGAME and cGAMES (up and downregulated) group when the genes in
527 those groups are put through IPA together. (* indicates that the activated or inhibited
528 indicator is registered from the IPAs based on the z-score for that regulator's expression
529 and not directly indicated based on software prediction).

530 **Discussion**

531 Identifying gene regulatory mechanisms activated by exercise during sensitive
532 developmental periods can aid in understanding how early-life exercise may promote a
533 "molecular memory" of exercise[23,60], via the epigenome, that informs long-term cell
534 function and behavioral outcomes. Here we present results demonstrating neuron-
535 specific, simultaneous characterization of translating mRNA and associated histone
536 modifications from a single population of hippocampal neurons obtained from ELE mice
537 to reveal molecular signatures of the early-life exercise experience. To our knowledge,
538 this is the first report describing use of the NuTRAP construct in a predominantly
539 neuronal population. Additionally, our unique experimental approach is a technical
540 advance for NuTRAP applications: by modifying the nuclear chromatin isolation
541 (INTACT) procedure to include cycloheximide, one can obtain both polyribosome-bound
542 mRNA (using TRAP) and nuclear DNA from a single lysate to directly correlate gene
543 expression programs with epigenetic regulatory mechanisms in the same set of cells. The
544 field of neuroepigenetics has been challenged by very limited approaches for coupling
545 cell-type specific transcriptional profiles with chromatin modifications without
546 compromising cell integrity (through flow sorting) or genomic coverage (through single-
547 cell sequencing). Therefore, the NuTRAP model offers an exciting opportunity to
548 overcome these challenges and perform paired transcriptomic and epigenomic analyses in
549 any brain cell type of interest for which a Cre line exists (cite other nutrap papers here).

550 Our study focuses on the impact of exercise on hippocampal gene expression and
551 associated epigenetic modifications specifically during juvenile – adolescent periods (the
552 fourth through sixth postnatal weeks of life in mice). We discover gene expression
553 programs, and alterations in the histone modifications H4K8ac and H3K27me3, that may
554 be unique to this early-life period. There have been recently published reports
555 investigating the effects of voluntary exercise on adolescent and adult hippocampal gene
556 expression and epigenetic modifications through RNA and DNA sequencing methods
557 from heterogenous cell populations[19,20]. In our study, several genes with either
558 chromatin-modifying or neurogenesis-regulating properties were either upregulated with
559 new H4K8ac (*Prox1*, *Sntb2*, and *Kptn*), or downregulated with new H3K27me3 (*Col3a1*,
560 *Efnb2*, *Epop*, and *Myoc*). For example, ELE could promote the expression of *Prox1* by

561 the addition of H4K8ac, and in turn, *Prox1* can promote neurogenic fate and cell location
562 assignment (such as DG granule cell fate over CA3 pyramidal cell identity[78]). ELE was
563 also found to alter the expression of *Kptn,* a gene encoding a protein involved in actin
564 dynamics and neuromorphogenesis[64]. Increased *Kptn* expression and accessibility may
565 possibly facilitate cytoskeletal changes occurring with altered synaptic plasticity after
566 exercise. Overall, the differentially expressed genes and their associated chromatin states
567 identified in this study provide molecular candidates involved in the effects of ELE on
568 hippocampal function.
569 Traditional epigenetic and gene expression analyses of bulk hippocampal tissue
570 are confounded by the cellular heterogeneity of the samples. Further, current methods for
571 paired analysis of the epigenome and transcriptome are restricted by the need for multiple
572 transgenic animal models or the use of highly expensive single-cell sequencing
573 technologies. However, it is critical to obtain epigenomic information in a cell-type
574 specific manner because there are unique epigenetic modifications distinguishing cell
575 subtypes of the central nervous system[10,79]. Roh et al. first developed the NuTRAP mouse
576 to characterize adipocyte-specific and hepatocyte-specific epigenetic and transcriptional
577 profiles[30]. The NuTRAP mouse has since been used to perform paired transcriptome and
578 DNA modification analysis in astrocytes and microglia, demonstrating its utility in CNS
579 cell-types[40]. The Emx1-NuTRAP mouse described here provides rapid, cost-effective
580 characterization of neuron-specific changes to epigenetic state and gene expression using
581 whole-tissue homogenates containing multiple cell types. In our technical validation
582 experiments, the SIT procedure produced high quality RNA and DNA of sufficient
583 concentration for downstream sequencing studies from a single mouse hippocampus.
584 This method effectively increases the total sample size used for each analysis as the tissue
585 sample does not need to be separated for DNA and RNA isolation. CUT&RUN and
586 CUT&Tag allow for low-input cell-specific chromatin analysis[61,80] further reducing the
587 required amount of starting material. Indeed, the DNA obtained from SIT could be used
588 for other applications for evaluating the chromatin landscape, including ATAC-seq.
589 A common approach to paired transcriptomic and epigenomic analyses is to use
590 separate brain tissue from one hemisphere for gene expression studies and the other side
591 for epigenetic analyses[81]. A previous study utilizing the NuTRAP allele in non-neuronal

592 brain cells used separate brain hemispheres to perform INTACT and TRAP[82]. However,
593 this assumes that cells of the same type from each half of the tissue will show the same
594 epigenetic and transcriptional profile. This is not necessarily the case for all cell types,
595 especially in the CNS, as structures of the brain can show high degrees of hemispheric
596 specialization[83-87]. To address the degree of transcriptional or epigenetic difference
597 between hippocampi from opposite hemispheres, we performed separate INTACT and
598 TRAP isolations using hippocampal tissue from one hemisphere for DNA isolation and
599 the contralateral hippocampus for mRNA isolation. We found that although differential
600 gene expression and histone modifications differed between left and right hippocampi,
601 functional analysis using gene ontology revealed similar biological processes between the
602 two sides.

603 Transcription is required for both hippocampal memory and LTP, a synaptic
604 plasticity response considered as the cellular correlate of learning and memory[88]. We
605 found that ELE can facilitate long-term memory formation in the hippocampus[17]. We
606 hypothesize that this may be due to altering the epigenomic landscape to promote a
607 transcriptional state supporting memory consolidation. In adult rodents, long-term
608 memory is formed in response to a subthreshold learning event after exercise or HDAC
609 inhibition and involves acetylation of neuroplasticity gene promoters[22]. Our study relates
610 this finding to the adolescent mouse brain and identifies new gene expression networks
611 and their epigenetic regulation likely involved in the hippocampal memory benefits of
612 ELE. We also identified a group of genes, cGAMS, that are altered in their gene
613 expression only in sedentary animals undergoing a threshold learning event. The
614 separation of this group from the cGAME and cGAMES groups indicates that ELE may
615 engage a separate network of genes to promote memory consolidation.

616 A next step of this work will be to test the necessity and sufficiency of the
617 identified gene networks, their histone modifications, and/or their upstream regulators
618 mediating the effects of ELE on hippocampal memory performance. Another unanswered
619 question is whether the effects of ELE on hippocampal memory persist well after
620 exercise cessation, and whether there is stability of ELE-induced epigenetic
621 modifications to allow for the persistence of ELE effects.

622 In summary, our work reveals ELE-induced transcriptomic and epigenomic
623 signatures in hippocampal neurons using the Emx1-NuTRAP mouse for such
624 comparisons. Presently, the field of neuroepigenetics is shifting to single-cell resolution
625 for sequencing studies. Our study was performed in bulk tissue enriched for neurons. As
626 the goal of this work was to characterize the transcriptional and epigenomic effects of
627 early-life exercise, cell subtype identity (as is often a priority in single-cell approaches)
628 was not necessary for tour initial hypotheses but would offer a second layer of
629 complexity to address this study's questions. Single-cell approaches can bias against
630 lowly-expressed genes, which presents the risk of not capturing small expression changes
631 in rate-limiting genes that may have large changes in function as a result of ELE. A
632 limiting factor for the use of the NuTRAP transgenic mouse is the requirement of a Cre
633 line to exist for the experimenter's cell type of interest. In our Emx1-NuTRAP model the
634 Cre-recombinase in Emx1 expressing cells is constitutively expressed, and this may
635 present off-target effects when present during development. Despite this, our study uses a
636 feasible, previously undescribed approach in the field of neuroepigenetics to pair
637 transcriptomic and epigenomic sequencing results from a population of hippocampal
638 neurons. Our approach revealed new molecular epigenetic candidates for further
639 mechanistic studies to examine the effects of early-life exercise on hippocampal function.
640 Furthermore, understanding how exercise uniquely impacts neuronal function during
641 juvenile-adolescent developmental periods could provide insights into an early-life
642 epigenetic memory of the ELE experience, revealing possible targets for improving
643 memory function or mitigating memory deficits in the setting of early-life cognitive and
644 neurodevelopmental disorders[89].
645
646 **Acknowledgements**
647 This work was supported by the National Institute of Neurological Disorders and Stroke
648 of the National Institutes of Health, under award number K12NS098482, the Conte
649 Center @ UCI Seed Grant, UC Irvine Institute for Clinical and Translational Sciences
650 Pilot Award, and the Robert Wood Johnson Foundation Amos Medical Faculty
651 Development Program (awarded to A.S.I.). We thank the UC Irvine School of Medicine,
652 Departments of Pediatrics for support. We would also like to thank Dr. Marcelo Wood

for scientific discussions and critical input on the project, and Drs. Melanie Oakes and Jenny Wu of the UC Irvine Genomics High Throughput Sequencing Facility for next generation sequencing experiments support.

Author Contributions

A.M.R., T.D.F., N.E.N. and A.S.I. designed the studies and interpreted the results. A.M.R., T.D.F., and A.S.I. performed INTACT and TRAP studies. A.M.R. built libraries for RNA-sequencing. N.E.N. performed CUT&RUN-seq experiments and built libraries for sequencing. N.E.N. and A.S.I. performed flow cytometry experiments. A.M.R. and A.S.I. performed immunostainings and immunofluorescent imaging. D.A.V. and A.B. built exercise cages and monitored running behavior. A.M.R. performed all bioinformatic analysis of sequencing data. A.M.R. and N.E.N. analyzed sequencing data, performed GO, GSEA and IPA analyses, and all other downstream analyses except where noted. A.S.I. performed behavioral studies. T.D.F. performed Spearman's correlations and gene length by fold change analysis. T.D.F. performed qPCR. N.E.N. designed the figures. A.M.R., T.D.F., and A.S.I. wrote and edited the manuscript, with N.E.N. providing edits to the manuscript. All authors discussed the results and edited and approved the manuscript.

Competing Interests

The authors declare no competing financial interests.

674 **Methods**

675 **Resource Availability**

676 ***Lead Contact***

677 Further information and requests for resources and reagents should be directed to and will
678 be fulfilled by the lead contact, Dr. Autumn Ivy (aivy@uci.edu)

679

680 ***Materials Availability***

681 - No new reagents or materials were generated for this study.
682 - The mouse lines used for this study are available from Jackson Labs (Emx1-
683 IRES-*Cre* knock-in mice, Jackson Laboratory Stock No: 005628, and NuTRAP
684 mice, Jackson Laboratory Stock No: 029899).

685

686 ***Animals***

687 Emx1-IRES-*Cre* knock-in mice (Jackson Laboratory Stock No: 005628),
688 NuTRAP mice (Jackson Laboratory Stock No: 029899), and C57Bl6/J (Jackson
689 Laboratory Stock No: 000664) wild-type mice were obtained from Jackson Laboratories.
690 Female Emx1-IRES-*Cre* and male NuTRAP mice were crossed to generate the Emx1-
691 NuTRAP mice used for this study. Mice were given free access to food and water, and
692 lights were maintained on a standard 12-hour light/dark cycle. On postnatal day (P) 21,
693 mice were weaned and pair-housed in either standard bedding cages or cages equipped
694 with a running wheel. Only male mice were used for the studies performed. Experiments
695 were conducted according to US National Institutes of Health guidelines for animal care
696 and use and were approved by the Institutional Animal Care and Use Committee of the
697 University of California, Irvine.

698

699 ***Behavior***

700 Wild-type mice were habituated, handled and then underwent OLM training[90] for
701 either three or ten minutes at P41 as described previously[17]. On postnatal day 36, mice
702 were brought into a testing room with reduced room brightness. Mice were handled for
703 approximately 2 min each, for a total of 5 consecutive days prior to the OLM training
704 session (twice a day for the first 2 days followed by once a day for the next 3 days).

705 Habituation sessions were 5 min, twice per day for 3 days (P39-P41) and occurred within
706 chambers containing four unique spatial cues on each wall of the chamber (horizontal
707 lines, black X, vertical strip, and blank wall). Habituation overlapped with the last 3 days
708 of handling. During the training phase (P42), mice were placed into the same chambers
709 with two identical objects and exposed to either a subthreshold (3 min) or threshold (10
710 min) training period. Mice were sacrificed for consolidation experiments 1 hour later.
711
712 ***Exercise Paradigm***
713 After weaning on P21, male mice from the same litters were randomly divided
714 and pair-housed in either standard cages without a wheel or cages equipped with a
715 stainless-steel running wheel similar to methods already described[17]. Animals housed
716 with running wheels had free access to the wheels from P21–41. Real-time data
717 acquisition (Vital View Software) was used to track distance ran recorded by magnetic
718 sensors that detect wheel revolutions. Each monitored wheel tracked running distance for
719 the entire cage (two mice per cage). Revolutions were quantified for every minute daily
720 for the duration of the exercise period and converted to distance ran per cage (km).
721 Exercised mice that underwent OLM training were individually tracked as described in
722 Valientes et al. 2021[91].
723
724 ***"SIT"***
725 On P42 both ELE and sedentary control (n=4/group) mice were sacrificed by rapid
726 cervical dislocation and both hemispheres of the hippocampus were dissected out and
727 collected for tissue processing. Hippocampal tissue samples were mechanically
728 homogenized in 1mL of nuclear preparation buffer (NPB) (10mM HEPES (pH7.5);
729 1.5mM MgCl2; 10mM KCl; 250mM sucrose; 0.1% IGEPAL CA-630; 0.2mM DTT;
730 100µg/mL cycloheximide; 1x Complete EDTA-free protease inhibitor (Roche)) by razor
731 blade. Samples were then triturated with an 18G needle and syringe 50x on ice.
732 Homogenized tissue samples were pipetted slowly onto 100µm cell strainer caps on
733 5mL tubes and centrifuged at 1,000rcf for 10 minutes at 4ºC. Cell pellets were
734 resuspended, and samples were pipetted onto 40µm cell strainer caps on 5mL tubes and
735 centrifuged at 1,000rcf for 10 minutes at 4ºC. For nuclear isolation, 100µL of

736 Streptavidin-coated Dynabeads were washed twice with 1mL NPB and resuspended with
737 100µL NPB. Cell pellets were resuspended and added to washed Streptavidin-coated
738 Dynabeads. Samples were briefly pipetted to thoroughly suspend the beads and incubated
739 on ice for 20 minutes. Samples were placed on a magnetic stand to pull down nuclei
740 bound to the beads. The supernatant from each sample was slowly pipetted off the beads
741 and transferred to new 1.5mL tubes for RNA isolation (described later). Nuclei-bound
742 beads were washed twice with 1mL INTACT buffer (10mM HEPES (pH7.5); 1.5mM
743 MgCl2; 10mM KCl; 250mM sucrose; 0.1% IGEPAL CA-630; 1x Complete EDTA-free
744 protease inhibitor (Roche)) and resuspended in 100µL INTACT buffer. Bead-bound
745 nuclei were flash frozen on dry ice and stored at -80ºC until ready for CUT&RUN
746 chromatin digestion and DNA purification.
747 For RNA isolation, 100µL of concentrated TRAP isolation buffer (10mM HEPES
748 (pH 7.5); 117mM MgCl2; 1M KCl; 10% IGEPAL CA-630; 100µg/mL cycloheximide;
749 11mg/mL sodium heparin; 20mM DTT; 2.2units/µL Rnasin; 1x Complete EDTA-free
750 protease inhibitor (Roche)) was added to each sample (supernatant above). Samples were
751 mixed by gentle pipetting and centrifuged at 16,000rcf for 10 minutes at 4ºC. The
752 supernatant from each sample was transferred to new 1.5mL tubes and 50µL of protein-G
753 Dynabeads was added to each sample. (To bind anti-GFP, 100µL of protein-G
754 Dynabeads were washed twice with 500µL NPB and resuspended to a final 100µL
755 volume. 2µL anti-GFP antibody (Sigma-Aldrich, G6539, Lot:128M4867V) was added to
756 each tube and incubated for 1 hour on a rotating nutator at 4ºC. Excess anti-GFP was
757 washed off with 200µL NPB and beads were resuspended in a final 100µL volume.)
758 Samples were incubated for 3 hours on a rotating nutator at 4ºC. Beads were washed 3x
759 in 1mL high salt wash buffer (HSWB) (50mM Tris (pH 7.5); 12mM MgCl2; 300mM
760 KCl; 1% IGEPAL CA-630; 2mM DTT; 100µg/mL cycloheximide) at 4ºC. After the third
761 wash the beads were slowly resuspended in 350µL RLT buffer (from Qiagen RNeasy
762 Mini kit #74004) by slowly pipetting up and down and incubated on a rotating nutator for
763 30 minutes at room temperature. Samples were placed on a magnetic stand to pull down
764 the beads, and the supernatant from each were transferred to new 1.5mL tubes and stored
765 at -80ºC until ready for RNA purification.
766

767 ***Separate TRAP RNA Isolation***

768 On P42, mice (n=3 mice/group) were sacrificed and the hippocampus was
769 dissected out as described above. Either the left or right brain hemisphere of the
770 hippocampus was processed for TRAP RNA isolation using methods similar to those
771 previously described[29,92] and the other hemisphere was processed for INTACT nuclear
772 isolation (see below). Hippocampal tissue was homogenized with a motorized pestle in
773 1ml of TRAP homogenization buffer (50mM Tris, (pH 7.5); 12mM $MgCl_2$; 100mM KCl;
774 1% NP-40; 100µg/ml cycloheximide; 1mg/ml sodium heparin; 2mM DTT; 0.2units/µl
775 RNasin; 1x Complete EDTA-free protease inhibitor (Roche)). Samples were centrifuged
776 at 16,000rcf for 10 minutes at 4ºC. The supernatant from each sample was collected and
777 incubated with 50µL of protein G Dynabeads (washed twice in 1mL TRAP
778 homogenization buffer without RNasin or protease inhibitor and resuspended in 50µL of
779 the same buffer). Samples were incubated for 30 minutes on a rotating nutator at 4ºC.
780 Following the incubation, 100µL of anti-GFP bound protein-G Dynabeads was added to
781 each sample. (To bind anti-GFP, 100µL of protein-G Dynabeads were washed twice with
782 500µL TRAP homogenization buffer without RNasin or protease inhibitor and
783 resuspended to a final 100µL volume. 2µL anti-GFP antibody (Sigma-Aldrich, G6539,
784 Lot:128M4867V) was added to each tube and incubated for 1 hour on a rotating nutator
785 at 4ºC. Excess anti-GFP was washed off with 200µL TRAP homogenization buffer
786 without RNasin or protease inhibitor and beads were resuspended in a final 100µL
787 volume.) Samples were incubated for 3 hours on a rotating nutator at 4ºC. Beads were
788 washed 3x in 1mL HSWB at 4ºC. After the final wash, the beads were resuspended in
789 350µL RLT buffer (from Qiagen RNeasy Mini kit #74004) and incubated on a rotating
790 nutator for 30 minutes at room temperature. Following the incubation, samples were
791 transferred to new 1.5mL tubes and stored at -80ºC until ready for RNA purification.
792

793 ***Separate INTACT Nuclear Isolation***

794 The remaining hippocampal hemisphere from each mouse (not used for TRAP
795 RNA isolation above) was processed for INTACT DNA isolation using methods similar
796 to those described[29,93]. Tissue samples were quickly chopped with a razor blade, added to
797 1mL of INTACT buffer, and triturated with an 18G needle and syringe 50x on ice.

798 Samples were then added onto 100µm cell strainer caps on 5mL tubes and centrifuged at
799 1,000rcf for 10 minutes at 4ºC. Cell pellets were resuspended and samples were pipetted
800 onto 40µm cell strainer caps and centrifuged at 1,000rcf for 10 minutes at 4ºC. 100µL of
801 streptavidin coated Dynabeads (washed twice with 1mL INTACT buffer and resuspended
802 to a final 100 µL volume) were added to each sample, and samples were incubated on ice
803 for 20 minutes. After incubation, nuclei bound beads were washed twice with 1mL and
804 resuspended in 100µL INTACT buffer. Bead-bound nuclei were flash frozen on dry ice
805 and stored at -80ºC until ready for CUT&RUN chromatin digestion and DNA
806 purification.
807
808 ***RNA Purification and Sequencing Library Preparation***
809 RNA was purified using the Qiagen RNeasy kit according to the manufacturer's
810 protocol. After purification, RNA quantity and quality were checked using the Qubit
811 RNA High Sensitivity assay and Agilent Bioanalyzer's Eukaryote Total RNA Pico assay,
812 respectively, at the University of California, Irvine Genomics High Throughput Facility
813 (UCI GHTF). Using an input of 15ng of total RNA, mRNA was isolated using
814 NEXTFLEX Poly(A) Beads 2.0, and the mRNA sequencing libraries were generated
815 using the NEXTFLEX Rapid Directional RNA-Seq Kit 2.0 according to the
816 manufacturer's instructions. Final libraries were sent to the UCI GHTF for Qubit dsDNA
817 High Sensitivity assay and the Agilent Bioanalyzer DNA High Sensitivity assay to
818 determine the quantity and quality of the RNA-seq libraries, respectively. Libraries were
819 sequenced at the UCI GHTF using 100bp paired end reads on a single lane of an Illumina
820 NovaSeq6000 to a minimum sequencing depth of 50 million reads.
821
822 ***Dorsal Hippocampal RNA Isolation***
823 P42 wild-type male mice were sacrificed by cervical dislocation. Left dorsal
824 hippocampus was extracted by bisecting the isolated hippocampus. The tissue was
825 homogenized and RNA was extracted using the Qiagen RNeasy kit according to the
826 manufacturer's protocol. Sequencing libraries were prepared from the RNA as described
827 under RNA purification and sequencing library preparation above except that ERCC

828 ExFold RNA Spike-In Mixes (ThermoFisher cat. 4465739) were added according to the
829 manufacturer's instructions.
830
831 ***Cleavage Under Target and Release Using Nuclease (CUT&RUN)***
832 For chromatin analysis, CUT&RUN was performed using the EpiCypher
833 CUTANA CUT&RUN protocol with slight modifications similar to what has already
834 been described[37]. Nuclei bound to beads were thawed and pulled down on a magnetic
835 stand. The supernatant was removed and beads were resuspended in 200µL wash buffer
836 (20mM HEPES (pH 7.5); 150mM NaCl; 0.5mM spermidine; 1x Complete EDTA-free
837 protease inhibitor (Roche)). Each sample was divided into three aliquots (50µL for anti-
838 H3K27me3 (Cell Signaling Technologies, C36B11, Lot: 16), 100µL for anti-H4K8ac
839 (Epicypher, 13-0047, Lot: 20202001-11), and 50µL for anti-IgG control (Rabbit IgG
840 Fisher Scientific, 026102)). Beads were pulled down on a magnetic stand, resuspended in
841 100µL wash buffer and incubated for 10 minutes at room temperature. After incubation
842 the beads were pulled down, the supernatant was removed, and the beads were
843 resuspended in 50µL ice cold antibody buffer (20mM HEPES (pH 7.5); 150mM NaCl;
844 0.5mM spermidine; 0.001mM digitonin; 2mM EDTA; 1x Complete EDTA-free protease
845 inhibitor (Roche)). 0.5µL of the appropriate antibody was added to each sample, and the
846 samples were mixed by gentle pipetting prior to overnight incubation at 4ºC on a nutator.
847 On the second day, the beads were pulled down on a magnetic stand, the
848 supernatant was removed and the beads were washed twice in 250µL ice cold wash
849 buffer with 0.001% digitonin. After the washes, beads were resuspended in 50µL ice cold
850 wash buffer with 0.001% digitonin, and 2.5µL of CUTANA pAG-MNase was added to
851 each sample and mixed by gentle pipetting. Samples were incubated for 10 minutes at
852 room temperature and beads were pulled down on a magnetic stand. The supernatant was
853 removed, and the beads were washed twice in 250µL ice cold wash buffer with 0.001%
854 digitonin and resuspended in 50µL of the same. 1µL of 100mM $CaCl_2$ was added to each
855 sample and mixed by gentle pipetting. Samples were incubated for 2 hours on a nutator at
856 4ºC. Following the incubation, 33µL of stop buffer (340mM NaCl; 20mM EDTA; 4mM
857 EGTA; 50µg/mL RNase A; 50µg/mL Glycogen) and 1.65µL of Spike-In DNA (Cell
858 Signaling Technology, #40366) was added to each sample. Samples were incubated in a

859 preheated thermocycler for 10 minutes at 37ºC. After incubation, samples were
860 transferred to new 1.5mL tubes and immediately processed for DNA purification.
861
862 ***DNA Purification and Library Preparation***
863 DNA was purified using the Monarch PCR and DNA cleanup kit (New England
864 Biolabs, 13-0041) according to the manufacturer's instructions. After purification, DNA
865 fragments were used to generate sequencing libraries using the NEXTFLEX Rapid DNA-
866 Seq Kit 2.0 according to the manufacturer's instructions. Indices were diluted to a final
867 concentration of 1:1,000 before being added to samples, and a total of 13 PCR cycles was
868 used for DNA amplification of the libraries. Final libraries were sent to the UCI GHTF
869 for Qubit dsDNA High Sensitivity assay and the Agilent Bioanalyzer DNA High
870 Sensitivity assay to determine the quantity and quality of the CUT&RUN-seq libraries,
871 respectively. Libraries were sequenced at the UCI GHTF using 100bp paired end reads
872 on a single lane of an Illumina NovaSeq6000 to a minimum sequencing depth of 10
873 million reads.
874
875 ***qPCR***
876 cDNA was generated from TRAP-isolated and total input RNA samples (n=2
877 samples/group) using the Transcriptor First Strand cDNA Synthesis Kit (Roche)
878 following the manufacturer's instructions. Relative gene expression for *Aqp4* (F: 5'-
879 ATCCAGCTCGATCTTTTGGA -3', R: 5'-TGAGCTCCACATCAGGACAG -3'),
880 *Tubb3* (F: 5'-GTCTCTAGCCGCGTGAAGTC -3', R: 5'-
881 GCAGGTCTGAGTCCCCTACA -3'), *Cd11b* (F: 5'-CCCATGACCTTCCAAGAGAA -
882 3', R: 5'-ACACTGGTAGAGGGCACCTG -3'), and *Mog* (F: 5'-
883 AAGAGGCAGCAATGGAGTTG -3', R: 5'-GACCTGCAGGAGGATCGTAG -3') was
884 determined by qPCR using FastStart Essential DNA Green Master Mix (Roche,
885 06402712001) following the manufacturer's protocol. Cycle counts for mRNA
886 quantification were normalized to *Gapdh* (F: 5'-CGTCCCGTAGACAAAATGGT -3', R:
887 5'-GAATTTGCCGTGAGTGGAGT -3'). Quantification was performed using the Pfaffl
888 method [94].
889

890 ***Immunofluoresence***

891 Emx1-NuTRAP mice were anesthetized intraperitoneally with 50mg/kg of
892 sodium pentobarbital and transfused transcardially with 4% paraformaldehyde (PFA) in
893 1x PBS. After perfusion, whole brains were dissected out and incubated in 4% PFA
894 overnight at 4ºC. After fixation, brains were incubated in 30% sucrose for 72 hours and
895 mounted in optimal cutting temperature (OCT) compound. 50µm coronal sections were
896 sliced through the hippocampus using a microtome, and every tenth section was collected
897 in 1mL of cryoprotectant and stored at -20ºC until ready for immunofluorescent labeling.
898 For immunofluorescence, sections were brought up to room temperature and washed 2x
899 in 1x PBS on a nutator for 5 minutes each. Sections were then washed 3x in 1x PBS with
900 0.3% triton-X. After washes, sections were incubated with mCherry polyclonal antibody
901 (ThermoFisher, PA5-34974, Lot: UG2804409F) at a 1:200 dilution in blocking solution
902 (1x PBS with 1% BSA) overnight at 4ºC on a nutator. The following day, sections were
903 washed 3x in 1x PBS. Sections were incubated for two hours at room temperature with
904 goat anti-rabbit Alexa Fluor 594 secondary antibody (Invitrogen, A-11012, Lot:
905 2119134) at a 1:200 dilution in blocking solution. After incubation, the sections were
906 washed twice in 1x PBS. To label nuclei, sections were incubated with DAPI at a
907 1:10,000 dilution in 1x PBS for 20 minutes. Sections were then washed 3x in 1x PBS and
908 cover slipped with Vectatshield®. Fluorescent images were acquired using a Keyence
909 BZ-X810 All-in-One Fluorescence microscope using the optical sectioning module.
910

911 ***Fluorescence Activated Cell Sorting***

912 Fluorescence activated cell sorting (FACS) was performed to characterize
913 neuronal and astrocytic NuTRAP cassette expression. Whole hippocampal tissue from
914 Emx1-NuTRAP mice was isolated and single-cell suspensions were immunostained for
915 cytometric analysis, as previously described[95]. We used antibodies for THY-1 (OX7)
916 AlexaFluor™ 647 (Santa Cruz Biotechnology, sc-53116 AF647, Lot: F2716;
917 concentration: 1:50) and S100β (Abcam, ab41548, Lot:GR3326165-1; concentration:
918 1:200) with an AlexaFluor™ 405 goat anti-rabbit IgG (H+L) (Invitrogen, A31556, Lot:
919 2273716; concentration:1:800) secondary antibody. FACS analysis was performed using
920 a BD FACSAria™ Fusion Flow Cytometer (BD Biosciences) at the University of

921 California, Irvine Stem Cell Core. Samples and single-stain controls were analyzed using
922 the FlowJo v10.8.1 software (BD Biosciences). Samples and controls were positively
923 gated for live cells (SSC-A and FSC-A) and single cells (FSC-H and FSC-A), and
924 negatively gated for autofluorescence (Comp-Alexa Fluor 647-A (Thy1) and Comp-
925 BV421-A (S100β)). Fraction of GFP+ neuronal cells was determined using quartile
926 analysis of Thy-1 and Comp-GFP-A (GFP). Fraction of GFP+ astrocytic cells was
927 determined using quartile analysis of S100β and Comp-GFP-A (GFP).
928
929 ***Bioinformatics Analysis***
930 *Reference assembly*: For all sequencing analysis that required it, the primary
931 reference assembly used was Genome Reference Consortium Mouse Build 38 patch
932 release 6 (GRCm38.p6).
933 *RNA-seq analysis*: FastQ files were quality checked for sequencing errors using
934 FastQC (version 0.11.9)[96]. No files were found to have sufficient quality errors to
935 discount their use. Files were aligned using STAR Aligner (version 2.7.3a)[97]. Duplicate
936 reads were removed using Picard Tools (version 1.87)[98]. SAM Tools was used to convert
937 BAM files to SAM files for use in downstream analysis. FastQC, alignment and duplicate
938 removal were all preformed on the High-Powered Compute Cluster (HPC3) operated by
939 The Research Cyberinfrastructure Center (RCIC) at the University of California, Irvine.
940 R (version 4.1.0)[99] was used for differentially expressed genes (DEG) analysis. Genomic
941 Alignments (version 1.28.0)[100] (summarizeOverlaps mode="IntersectionNotEmpty",
942 singleEnd=FALSE, ignore.strand=FALSE, fragments=TRUE), Genomic Features
943 (version 1.44.0) (exons by gene), and R SAM Tools (version 2.8.0)[101]
944 (yieldSize=100000) were used to extract a count matrix and generate a summarized
945 experiment object. DEseq2 (version 1.32.0)[102] was used to perform a DEG analysis.
946 Ensemble IDs were converted to gene symbols using BiomaRt (version 2.48.1)[103,104].
947 PCA plots using the top 2000 genes were generated using ggplot2 (version 3.3.4)[105].
948 Samples were determined as outliers if the variability between the samples heavily
949 weighted PC1 to those samples. This excluded 2 sedentary samples and 1 ELE sample.
950 Heatmaps were generated using gplots (version 3.1.1)[106] and RColorBrewer (version1.1-
951 2)[107]. Volcano Plots were generated using ggplot2[105]. Venn diagrams were generated

952 using the Venn diagram tool from Bioinformatics and Evolutionary Genomics[108]. Gene
953 ontology analysis was performed using Panther Classification System (version 16.0)[44].
954 Genes were also categorized and a leading edge heatmap was also generated using Gene
955 Set Enrichment Analysis (version GSEA 4.1.0)[55]. Upstream regulators were identified
956 from the DEGs upregulated by ELE using Qiagen's Ingenuity Pathway Analysis (IPA)
957 (Fall 2021 Release)[45].
958 *CUT&RUN-seq analysis*: FastQ files were quality checked for sequencing errors
959 using FastQC (version 0.11.9)[96]. No files were found to have sufficient quality errors to
960 discount their use. FastQ files were aligned using Bowtie2 (version 2.4.1)[109]. Significant
961 peaks were called from these aligned files using SEACR, developed in CUT&Tag for
962 efficient epigenomic profiling of small samples and single cells[61,109], according to
963 CUT&Tag Data Processing and Analysis Tutorial (updated August 12 2020):
964 https://www.protocols.io/view/cut-amp-tag-data-processing-and-analysis-tutorial-
965 bjk2kky. An FDR higher than 0.1 was considered too high for called peaks. This
966 threshold excluded 4 samples (3 ELE H4K8ac separate isolation samples and 1 ELE
967 H4K8ac SIT sample). Peaks were called using the stringent and 0.01 settings. Significant
968 peaks were annotated using ChIPseeker (version 1.8.6)[110] using
969 TxDb.Mmusculus.UCSC.mm10.knownGene[111] as a reference with the following settings:
970 tssRegion = c(-3000, 3000), TxDb = TxDb.Mmusculus.UCSC.mm10.knownGene, level
971 = "transcript", assignGenomicAnnotation = TRUE, genomicAnnotationPriority =
972 c("Promoter", "5UTR", "3UTR", "Exon", "Intron", "Downstream", "Intergenic"), annoDb
973 = NULL, addFlankGeneInfo = FALSE, flankDistance = 5000, sameStrand = FALSE,
974 ignoreOverlap = FALSE, ignoreUpstream = FALSE, ignoreDownstream = FALSE,
975 overlap = "TSS", verbose = TRUE). This approach annotated peaks to the closest gene by
976 distance from the promoter, except if that peak falls within a gene before the distal
977 intergenic region. Ensemble IDs were converted to gene symbols using BiomaRt[103,104].
978 Gene lists of peaks present in each condition were used to generate Venn diagrams, as
979 with RNA-seq analysis[108]. Further Venn diagrams were generated comparing DEGs with
980 peak calls. Peaks were visualized using UCSC Genome Browser and Genome Browser in
981 a Box[112-114].

982 Normalized counts (for read depth) at binned sections of the DNA as well as
983 RNA-seq gene expression count (normalized for read depth) were compared between
984 simultaneous and separate isolations as well as left and right hemispheres using
985 Spearman's correlations in R with the package ggpubr (version 0.4.0)[115]. Bar plots were
986 generated using Graph Pad 9 PRISM.
987
988 ***Data Availability***
989 RNA-seq and CUT&RUN-seq data will be deposited and publicly available as of
990 the date of publication. Accession numbers will be listed here pending publication. Any
991 additional information required to reanalyze the data reported in this paper is available
992 from the lead contact upon request.

References

1 Bedrosian, T. A., Quayle, C., Novaresi, N. & Gage, F. H. Early life experience drives structural variation of neural genomes in mice. *Science (New York, N.Y.)* **359**, 1395-1399, doi:10.1126/science.aah3378 (2018).

2 Stroud, H. *et al.* Early-Life Gene Expression in Neurons Modulates Lasting Epigenetic States. *Cell* **171**, 1151-1164.e1116, doi:https://doi.org/10.1016/j.cell.2017.09.047 (2017).

3 Herre, M. & Korb, E. The chromatin landscape of neuronal plasticity. *Curr Opin Neurobiol* **59**, 79-86, doi:10.1016/j.conb.2019.04.006 (2019).

4 Campbell, R. R. & Wood, M. A. How the epigenome integrates information and reshapes the synapse. *Nat Rev Neurosci* **20**, 133-147, doi:10.1038/s41583-019-0121-9 (2019).

5 Kronman, H. *et al.* Long-term behavioral and cell-type-specific molecular effects of early life stress are mediated by H3K79me2 dynamics in medium spiny neurons. *Nat Neurosci* **24**, 667-676, doi:10.1038/s41593-021-00814-8 (2021).

6 Sagarkar, S. *et al.* LSD1-BDNF activity in lateral hypothalamus-medial forebrain bundle area is essential for reward seeking behavior. *Progress in neurobiology* **202**, 102048, doi:10.1016/j.pneurobio.2021.102048 (2021).

7 Webb, W. M. *et al.* The SETD6 Methyltransferase Plays an Essential Role in Hippocampus-Dependent Memory Formation. *Biological psychiatry* **87**, 577-587, doi:10.1016/j.biopsych.2019.05.022 (2020).

8 Bolton, J. L. *et al.* Unexpected Transcriptional Programs Contribute to Hippocampal Memory Deficits and Neuronal Stunting after Early-Life Adversity. *Cell Rep* **33**, 108511, doi:10.1016/j.celrep.2020.108511 (2020).

9 Campbell, R. R. *et al.* HDAC3 Activity within the Nucleus Accumbens Regulates Cocaine-Induced Plasticity and Behavior in a Cell-Type-Specific Manner. *The Journal of neuroscience : the official journal of the Society for Neuroscience* **41**, 2814-2827, doi:10.1523/JNEUROSCI.2829-20.2021 (2021).

10 Lister, R. *et al.* Global Epigenomic Reconfiguration During Mammalian Brain Development. *Science* **341**, 1237905, doi:10.1126/science.1237905 (2013).

11 Lavery, L. A. & Zoghbi, H. Y. The distinct methylation landscape of maturing neurons and its role in Rett syndrome pathogenesis. *Current opinion in neurobiology* **59**, 180-188, doi:10.1016/j.conb.2019.08.001 (2019).

12 Aguilar, R., Bustos, F. J., Nardocci, G., van Zundert, B. & Montecino, M. Epigenetic silencing of the osteoblast-lineage gene program during hippocampal maturation. *Journal of cellular biochemistry* **122**, 367-384, doi:10.1002/jcb.29865 (2021).

13 West, A. E. & Greenberg, M. E. Neuronal activity-regulated gene transcription in synapse development and cognitive function. *Cold Spring Harbor perspectives in biology* **3**, doi:10.1101/cshperspect.a005744 (2011).

14 Bale, T. L. *et al.* Early life programming and neurodevelopmental disorders. *Biological psychiatry* **68**, 314-319, doi:10.1016/j.biopsych.2010.05.028 (2010).

15 Cotman, C. W., Berchtold, N. C. & Christie, L.-A. Exercise builds brain health: key roles of growth factor cascades and inflammation. *Trends in Neurosciences* **30**, 464-472, doi:https://doi.org/10.1016/j.tins.2007.06.011 (2007).

16 Voss, M. W., Vivar, C., Kramer, A. F. & van Praag, H. Bridging animal and human models of exercise-induced brain plasticity. *Trends in cognitive sciences* **17**, 525-544, doi:10.1016/j.tics.2013.08.001 (2013).

17 Ivy, A. S. *et al.* A Unique Mouse Model of Early Life Exercise Enables Hippocampal Memory and Synaptic Plasticity. *Scientific Reports* **10**, 9174, doi:10.1038/s41598-020-66116-4 (2020).

18 Berchtold, N. C., Castello, N. & Cotman, C. W. Exercise and time-dependent benefits to learning and memory. *Neuroscience* **167**, 588-597, doi:10.1016/j.neuroscience.2010.02.050 (2010).

19 Urdinguio, R. G. *et al.* Physical exercise shapes the mouse brain epigenome. *Mol Metab* **54**, 101398, doi:10.1016/j.molmet.2021.101398 (2021).

20 Abel, J. L. & Rissman, E. F. Running-induced epigenetic and gene expression changes in the adolescent brain. *International journal of developmental neuroscience : the official journal of the International Society for Developmental Neuroscience* **31**, 382-390, doi:10.1016/j.ijdevneu.2012.11.002 (2013).

21 Ieraci, A., Mallei, A., Musazzi, L. & Popoli, M. Physical exercise and acute restraint stress differentially modulate hippocampal brain-derived neurotrophic factor transcripts and epigenetic mechanisms in mice. *Hippocampus* **25**, 1380-1392, doi:10.1002/hipo.22458 (2015).

22 Intlekofer, K. A. *et al.* Exercise and Sodium Butyrate Transform a Subthreshold Learning Event into Long-Term Memory via a Brain-Derived Neurotrophic factor-Dependent Mechanism. *Neuropsychopharmacology* **38**, 2027-2034, doi:10.1038/npp.2013.104 (2013).

23 Butler, C. W. *et al.* Exercise opens a temporal window for enhanced cognitive improvement from subsequent physical activity. *Learn Mem* **26**, 485-492, doi:10.1101/lm.050278.119 (2019).

24 Titterness, A. K., Wiebe, E., Kwasnica, A., Keyes, G. & Christie, B. R. Voluntary exercise does not enhance long-term potentiation in the adolescent female dentate gyrus. *Neuroscience* **183**, 25-31, doi:10.1016/j.neuroscience.2011.03.050 (2011).

25 Gomes da Silva, S. & Arida, R. M. Physical activity and brain development. *Expert review of neurotherapeutics* **15**, 1041-1051, doi:10.1586/14737175.2015.1077115 (2015).

26 Gomes da Silva, S. *et al.* Early exercise promotes positive hippocampal plasticity and improves spatial memory in the adult life of rats. *Hippocampus* **22**, 347-358, doi:10.1002/hipo.20903 (2012).

27 Fernandes, J., Arida, R. M. & Gomez-Pinilla, F. Physical exercise as an epigenetic modulator of brain plasticity and cognition. *Neuroscience and biobehavioral reviews* **80**, 443-456, doi:10.1016/j.neubiorev.2017.06.012 (2017).

1083 28 Intlekofer, K. A. *et al.* Exercise and sodium butyrate transform a subthreshold
1084 learning event into long-term memory via a brain-derived neurotrophic
1085 factor-dependent mechanism. *Neuropsychopharmacology* **38**, 2027-2034,
1086 doi:10.1038/npp.2013.104 (2013).
1087 29 Roh, H. C. *et al.* Simultaneous Transcriptional and Epigenomic Profiling from
1088 Specific Cell Types within Heterogeneous Tissues In Vivo. *Cell Rep* **18**, 1048-
1089 1061, doi:10.1016/j.celrep.2016.12.087 (2017).
1090 30 Deal, R. B. & Henikoff, S. The INTACT method for cell type-specific gene
1091 expression and chromatin profiling in Arabidopsis thaliana. *Nature protocols*
1092 **6**, 56-68, doi:10.1038/nprot.2010.175 (2011).
1093 31 Heiman, M. *et al.* A translational profiling approach for the molecular
1094 characterization of CNS cell types. *Cell* **135**, 738-748,
1095 doi:10.1016/j.cell.2008.10.028 (2008).
1096 32 Gorski, J. A. *et al.* Cortical excitatory neurons and glia, but not GABAergic
1097 neurons, are produced in the Emx1-expressing lineage. *J Neurosci* **22**, 6309-
1098 6314, doi:10.1523/jneurosci.22-15-06309.2002 (2002).
1099 33 Chan, C. H. *et al.* Emx1 is a marker for pyramidal neurons of the cerebral
1100 cortex. *Cerebral cortex (New York, N.Y. : 1991)* **11**, 1191-1198,
1101 doi:10.1093/cercor/11.12.1191 (2001).
1102 34 Hong, S. M. *et al.* Reduced hippocampal neurogenesis and skill reaching
1103 performance in adult Emx1 mutant mice. *Experimental neurology* **206**, 24-32,
1104 doi:10.1016/j.expneurol.2007.03.028 (2007).
1105 35 Willaime-Morawek, S. & van der Kooy, D. Cortex- and striatum- derived
1106 neural stem cells produce distinct progeny in the olfactory bulb and striatum.
1107 *The European journal of neuroscience* **27**, 2354-2362, doi:10.1111/j.1460-
1108 9568.2008.06206.x (2008).
1109 36 Luo, L. *et al.* Optimizing Nervous System-Specific Gene Targeting with Cre
1110 Driver Lines: Prevalence of Germline Recombination and Influencing Factors.
1111 *Neuron* **106**, 37-65.e35, doi:10.1016/j.neuron.2020.01.008 (2020).
1112 37 Skene, P. J., Henikoff, J. G. & Henikoff, S. Targeted in situ genome-wide
1113 profiling with high efficiency for low cell numbers. *Nature protocols* **13**,
1114 1006-1019, doi:10.1038/nprot.2018.015 (2018).
1115 38 Liu, Y. *et al.* Glial fibrillary acidic protein-expressing neural progenitors give
1116 rise to immature neurons via early intermediate progenitors expressing both
1117 glial fibrillary acidic protein and neuronal markers in the adult hippocampus.
1118 *Neuroscience* **166**, 241-251, doi:10.1016/j.neuroscience.2009.12.026 (2010).
1119 39 Garcia, A. D. R., Doan, N. B., Imura, T., Bush, T. G. & Sofroniew, M. V. GFAP-
1120 expressing progenitors are the principal source of constitutive neurogenesis
1121 in adult mouse forebrain. *Nature Neuroscience* **7**, 1233-1241,
1122 doi:10.1038/nn1340 (2004).
1123 40 Chucair-Elliott, A. J. *et al.* Inducible cell-specific mouse models for paired
1124 epigenetic and transcriptomic studies of microglia and astroglia. *bioRxiv*,
1125 862722, doi:10.1101/862722 (2019).
1126 41 Jordan, J. T. The rodent hippocampus as a bilateral structure: A review of
1127 hemispheric lateralization. *Hippocampus* **30**, 278-292,
1128 doi:https://doi.org/10.1002/hipo.23188 (2020).

1129 42 Berchtold, N. C., Chinn, G., Chou, M., Kesslak, J. P. & Cotman, C. W. Exercise
1130 primes a molecular memory for brain-derived neurotrophic factor protein
1131 induction in the rat hippocampus. *Neuroscience* **133**, 853-861,
1132 doi:10.1016/j.neuroscience.2005.03.026 (2005).
1133 43 McNulty, S. E. *et al.* Differential roles for Nr4a1 and Nr4a2 in object location
1134 vs. object recognition long-term memory. *Learning & memory (Cold Spring*
1135 *Harbor, N.Y.)* **19**, 588-592, doi:10.1101/lm.026385.112 (2012).
1136 44 Mi, H. & Thomas, P. 123-140 (Humana Press, 2009).
1137 45 Krämer, A., Green, J., Pollard, J. & Tugendreich, S. Causal analysis approaches
1138 in Ingenuity Pathway Analysis. *Bioinformatics* **30**, 523-530,
1139 doi:10.1093/bioinformatics/btt703 (2014).
1140 46 Kandel, E. R. The molecular biology of memory: cAMP, PKA, CRE, CREB-1,
1141 CREB-2, and CPEB. *Molecular brain* **5**, 14, doi:10.1186/1756-6606-5-14
1142 (2012).
1143 47 Kerimoglu, C. *et al.* KMT2A and KMT2B Mediate Memory Function by
1144 Affecting Distinct Genomic Regions. *Cell reports* **20**, 538-548,
1145 doi:10.1016/j.celrep.2017.06.072 (2017).
1146 48 Ashbrook, D. G. *et al.* Transcript co-variance with Nestin in two mouse
1147 genetic reference populations identifies Lef1 as a novel candidate regulator
1148 of neural precursor cell proliferation in the adult hippocampus. *Front*
1149 *Neurosci* **8**, 418, doi:10.3389/fnins.2014.00418 (2014).
1150 49 Tapia-González, S., Muñoz, M., Cuartero, M. & Sánchez-Capelo, A. Smad3 is
1151 required for the survival of proliferative intermediate progenitor cells in the
1152 dentate gyrus of adult mice. *Cell Communication and Signaling* **11**, 93,
1153 doi:10.1186/1478-811x-11-93 (2013).
1154 50 Tiano, J. P., Springer, D. A. & Rane, S. G. SMAD3 Negatively Regulates Serum
1155 Irisin and Skeletal Muscle FNDC5 and Peroxisome Proliferator-activated
1156 Receptor γ Coactivator 1-α (PGC-1α) during Exercise. *Journal of Biological*
1157 *Chemistry* **290**, 7671-7684, doi:10.1074/jbc.m114.617399 (2015).
1158 51 Sun, Z. *et al.* EGR1 recruits TET1 to shape the brain methylome during
1159 development and upon neuronal activity. *Nature Communications* **10**,
1160 doi:10.1038/s41467-019-11905-3 (2019).
1161 52 Bouché, V. *et al.* Drosophila Mitf regulates the V-ATPase and the lysosomal-
1162 autophagic pathway. *Autophagy* **12**, 484-498,
1163 doi:10.1080/15548627.2015.1134081 (2016).
1164 53 Guan, Z. *et al.* Integration of long-term-memory-related synaptic plasticity
1165 involves bidirectional regulation of gene expression and chromatin structure.
1166 *Cell* **111**, 483-493, doi:10.1016/s0092-8674(02)01074-7 (2002).
1167 54 Korzus, E., Rosenfeld, M. G. & Mayford, M. CBP Histone Acetyltransferase
1168 Activity Is a Critical Component of Memory Consolidation. *Neuron* **42**, 961-
1169 972, doi:https://doi.org/10.1016/j.neuron.2004.06.002 (2004).
1170 55 Subramanian, A. *et al.* Gene set enrichment analysis: A knowledge-based
1171 approach for interpreting genome-wide expression profiles. *Proceedings of*
1172 *the National Academy of Sciences* **102**, 15545-15550,
1173 doi:10.1073/pnas.0506580102 (2005).

1174 56 Nofrini, V., Di Giacomo, D. & Mecucci, C. Nucleoporin genes in human
1175 diseases. *European Journal of Human Genetics* **24**, 1388-1395,
1176 doi:10.1038/ejhg.2016.25 (2016).
1177 57 Gomes-Duarte, A., Lacerda, R., Menezes, J. & Romão, L. eIF3: a factor for
1178 human health and disease. *RNA Biol* **15**, 26-34,
1179 doi:10.1080/15476286.2017.1391437 (2018).
1180 58 Alvarez-López, M. J. *et al.* Long-term exercise modulates hippocampal gene
1181 expression in senescent female mice. *J Alzheimers Dis* **33**, 1177-1190,
1182 doi:10.3233/jad-121264 (2013).
1183 59 Butler, A. A., Sanchez, R. G., Jarome, T. J., Webb, W. M. & Lubin, F. D. O-GlcNAc
1184 and EZH2-mediated epigenetic regulation of gene expression during
1185 consolidation of fear memories. *Learning & memory (Cold Spring Harbor,*
1186 *N.Y.)* **26**, 373-379, doi:10.1101/lm.049023.118 (2019).
1187 60 Butler, A. A., Sanchez, R. G., Jarome, T. J., Webb, W. M. & Lubin, F. D. O-GlcNAc
1188 and EZH2-mediated epigenetic regulation of gene expression during
1189 consolidation of fear memories. *Learning & memory (Cold Spring Harbor,*
1190 *N.Y.)* **26**, 373-379, doi:10.1101/lm.049023.118 (2019).
1191 61 Kaya-Okur, H. S. *et al.* CUT&Tag for efficient epigenomic profiling of small
1192 samples and single cells. *Nature Communications* **10**, doi:10.1038/s41467-
1193 019-09982-5 (2019).
1194 62 Stergiopoulos, A., Elkouris, M. & Politis, P. K. Prospero-related homeobox 1
1195 (Prox1) at the crossroads of diverse pathways during adult neural fate
1196 specification. *Front Cell Neurosci* **8**, 454, doi:10.3389/fncel.2014.00454
1197 (2014).
1198 63 Camp, N. D. *et al.* Individual protomers of a G protein-coupled receptor dimer
1199 integrate distinct functional modules. *Cell Discov* **1**, 15011-,
1200 doi:10.1038/celldisc.2015.11 (2015).
1201 64 Baple, E. L. *et al.* Mutations in KPTN cause macrocephaly,
1202 neurodevelopmental delay, and seizures. *Am J Hum Genet* **94**, 87-94,
1203 doi:10.1016/j.ajhg.2013.10.001 (2014).
1204 65 Peterson, M. D. & Titus, M. A. F-actin distribution of Dictyostelium myosin I
1205 double mutants. *J Eukaryot Microbiol* **41**, 652-657, doi:10.1111/j.1550-
1206 7408.1994.tb01529.x (1994).
1207 66 Johnson Chacko, L. *et al.* Transcriptome-Wide Analysis Reveals a Role for
1208 Extracellular Matrix and Integrin Receptor Genes in Otic Neurosensory
1209 Differentiation from Human iPSCs. *Int J Mol Sci* **22**,
1210 doi:10.3390/ijms221910849 (2021).
1211 67 Truter, S., Andrikopoulos, K., Di Liberto, M., Womack, L. & Ramirez, F. Pro-
1212 alpha 2(V) collagen gene; pairwise analysis of the amino-propeptide coding
1213 domain, and cross-species comparison of the promoter sequence. *Connect*
1214 *Tissue Res* **29**, 51-59, doi:10.3109/03008209309061966 (1993).
1215 68 Lévy, J. *et al.* EFNB2 haploinsufficiency causes a syndromic
1216 neurodevelopmental disorder. *Clin Genet* **93**, 1141-1147,
1217 doi:10.1111/cge.13234 (2018).

1218 69 Xiong, C. *et al.* Targeting Forward and Reverse EphB4/EFNB2 Signaling by a
1219 Peptide with Dual Functions. *Sci Rep* **10**, 520, doi:10.1038/s41598-020-
1220 57477-x (2020).
1221 70 Zhu, F. *et al.* EFNB2 facilitates cell proliferation, migration, and invasion in
1222 pancreatic ductal adenocarcinoma via the p53/p21 pathway and EMT.
1223 *Biomed Pharmacother* **125**, 109972, doi:10.1016/j.biopha.2020.109972
1224 (2020).
1225 71 Ferrari, K. J., Lavarone, E. & Pasini, D. The Dual Role of EPOP and Elongin BC
1226 in Controlling Transcriptional Activity. *Mol Cell* **64**, 637-638,
1227 doi:10.1016/j.molcel.2016.11.009 (2016).
1228 72 Liefke, R., Karwacki-Neisius, V. & Shi, Y. EPOP Interacts with Elongin BC and
1229 USP7 to Modulate the Chromatin Landscape. *Mol Cell* **64**, 659-672,
1230 doi:10.1016/j.molcel.2016.10.019 (2016).
1231 73 Warburton, E. C. *et al.* cAMP responsive element-binding protein
1232 phosphorylation is necessary for perirhinal long-term potentiation and
1233 recognition memory. *J Neurosci* **25**, 6296-6303, doi:10.1523/jneurosci.0506-
1234 05.2005 (2005).
1235 74 Logan, T., Bendor, J., Toupin, C., Thorn, K. & Edwards, R. H. α-Synuclein
1236 promotes dilation of the exocytotic fusion pore. *Nat Neurosci* **20**, 681-689,
1237 doi:10.1038/nn.4529 (2017).
1238 75 Fournier, A. E., GrandPre, T. & Strittmatter, S. M. Identification of a receptor
1239 mediating Nogo-66 inhibition of axonal regeneration. *Nature* **409**, 341-346,
1240 doi:10.1038/35053072 (2001).
1241 76 Pérez-Otaño, I., Larsen, R. S. & Wesseling, J. F. Emerging roles of GluN3-
1242 containing NMDA receptors in the CNS. *Nat Rev Neurosci* **17**, 623-635,
1243 doi:10.1038/nrn.2016.92 (2016).
1244 77 Chodelkova, O., Masek, J., Korinek, V., Kozmik, Z. & Machon, O. Tcf7L2 is
1245 essential for neurogenesis in the developing mouse neocortex. *Neural Dev* **13**,
1246 8, doi:10.1186/s13064-018-0107-8 (2018).
1247 78 Iwano, T., Masuda, A., Kiyonari, H., Enomoto, H. & Matsuzaki, F. Prox1
1248 postmitotically defines dentate gyrus cells by specifying granule cell identity
1249 over CA3 pyramidal cell fate in the hippocampus. *Development (Cambridge,*
1250 *England)* **139**, 3051-3062, doi:10.1242/dev.080002 (2012).
1251 79 Luo, C. *et al.* Single-cell methylomes identify neuronal subtypes and
1252 regulatory elements in mammalian cortex. *Science* **357**, 600-604,
1253 doi:10.1126/science.aan3351 (2017).
1254 80 Skene, P. J., Henikoff, J. G. & Henikoff, S. Targeted in situ genome-wide
1255 profiling with high efficiency for low cell numbers. *Nature protocols* **13**,
1256 1006-1019, doi:10.1038/nprot.2018.015 (2018).
1257 81 Helbling, J.-C., Kinouchi, K., Trifilieff, P., Sassone-Corsi, P. & Moisan, M.-P.
1258 Combined Gene Expression and Chromatin Immunoprecipitation From a
1259 Single Mouse Hippocampus. *Current Protocols* **1**, e33,
1260 doi:https://doi.org/10.1002/cpz1.33 (2021).
1261 82 Chucair-Elliott, A. J. *et al.* Inducible cell-specific mouse models for paired
1262 epigenetic and transcriptomic studies of microglia and astroglia. *Commun*
1263 *Biol* **3**, 693, doi:10.1038/s42003-020-01418-x (2020).

1264 83 Doty, R. W., Fei, R., Hu, S. & Kavcic, V. Long-term reversal of hemispheric
1265 specialization for visual memory in a split-brain macaque. *Behavioural brain*
1266 *research* **102**, 99-113, doi:10.1016/s0166-4328(99)00006-6 (1999).
1267 84 Duboc, V., Dufourcq, P., Blader, P. & Roussigné, M. Asymmetry of the Brain:
1268 Development and Implications. *Annual review of genetics* **49**, 647-672,
1269 doi:10.1146/annurev-genet-112414-055322 (2015).
1270 85 Güntürkün, O., Ströckens, F. & Ocklenburg, S. Brain Lateralization: A
1271 Comparative Perspective. *Physiological reviews* **100**, 1019-1063,
1272 doi:10.1152/physrev.00006.2019 (2020).
1273 86 Hubel, D. H. & Wiesel, T. N. Receptive fields, binocular interaction and
1274 functional architecture in the cat's visual cortex. *The Journal of Physiology*
1275 **160**, 106-154, doi:https://doi.org/10.1113/jphysiol.1962.sp006837 (1962).
1276 87 Spiers, H. J. *et al.* Unilateral temporal lobectomy patients show lateralized
1277 topographical and episodic memory deficits in a virtual town. *Brain : a*
1278 *journal of neurology* **124**, 2476-2489, doi:10.1093/brain/124.12.2476
1279 (2001).
1280 88 Lynch, M. A. Long-term potentiation and memory. *Physiological reviews* **84**,
1281 87-136, doi:10.1152/physrev.00014.2003 (2004).
1282 89 Achilly, N. P., Wang, W. & Zoghbi, H. Y. Presymptomatic training mitigates
1283 functional deficits in a mouse model of Rett syndrome. *Nature* **592**, 596-600,
1284 doi:10.1038/s41586-021-03369-7 (2021).
1285 90 Kwapis, J. L. *et al.* Epigenetic regulation of the circadian gene Per1
1286 contributes to age-related changes in hippocampal memory. *Nat Commun* **9**,
1287 3323, doi:10.1038/s41467-018-05868-0 (2018).
1288 91 David A Valientes, A. M. R., Autumn S Ivy. An Improved Method for Individual
1289 Tracking of Voluntary Wheel Running in Pair-housed Juvenile Mice. *BIO-*
1290 *PROTOCOL* **11**, doi:10.21769/bioprotoc.4071 (2021).
1291 92 Long, J. Z. *et al.* A smooth muscle-like origin for beige adipocytes. *Cell*
1292 *metabolism* **19**, 810-820, doi:10.1016/j.cmet.2014.03.025 (2014).
1293 93 Deal, R. B. & Henikoff, S. A simple method for gene expression and chromatin
1294 profiling of individual cell types within a tissue. *Developmental cell* **18**, 1030-
1295 1040, doi:10.1016/j.devcel.2010.05.013 (2010).
1296 94 Pfaffl, M. W. A new mathematical model for relative quantification in real-
1297 time RT-PCR. *Nucleic Acids Res* **29**, e45, doi:10.1093/nar/29.9.e45 (2001).
1298 95 Schwarz, J. M. Using fluorescence activated cell sorting to examine cell-type-
1299 specific gene expression in rat brain tissue. *Journal of visualized experiments :*
1300 *JoVE*, e52537, doi:10.3791/52537 (2015).
1301 96 FastQC v. 0.11.9 (Babraham Bioinformatics, 2005).
1302 97 Dobin, A. *et al.* STAR: ultrafast universal RNA-seq aligner. *Bioinformatics* **29**,
1303 15-21, doi:10.1093/bioinformatics/bts635 (2013).
1304 98 Picard v. 1.87 (Broad Institute, 2013).
1305 99 R (R Foundation for statistical Computing, Vienna, Austria, 2010).
1306 100 Lawrence, M. *et al.* Software for Computing and Annotating Genomic Ranges.
1307 *PLoS Computational Biology* **9**, e1003118, doi:10.1371/journal.pcbi.1003118
1308 (2013).

101 Rsamtools: Binary alignment (BAM), FASTA, variant call (BCF), and tabix file import (Bioconductor Bioconductor 2021).
102 Love, M. I., Huber, W. & Anders, S. Moderated estimation of fold change and dispersion for RNA-seq data with DESeq2. *Genome Biology* **15**, doi:10.1186/s13059-014-0550-8 (2014).
103 Durinck, S. *et al.* BioMart and Bioconductor: a powerful link between biological databases and microarray data analysis. *Bioinformatics* **21**, 3439-3440, doi:10.1093/bioinformatics/bti525 (2005).
104 Durinck, S., Spellman, P. T., Birney, E. & Huber, W. Mapping identifiers for the integration of genomic datasets with the R/Bioconductor package biomaRt. *Nature protocols* **4**, 1184-1191, doi:10.1038/nprot.2009.97 (2009).
105 Ggplot2: Elegant graphics for data analysis v. 3.3.4 (Springer International Publishing, Cham, Switzerland, 2016).
106 gplots: Various R Programming Tools for Plotting Data v. 3.1.1 (Tal Galili 2020).
107 RColorBrewer: ColorBrewer Palettes (Erich Neuwirth, CRAN, 2014).
108 Venn Diagram: Calculate and draw custom Venn diagrams (BELGIUM, 2021).
109 Langmead, B. & Salzberg, S. L. Fast gapped-read alignment with Bowtie 2. *Nature Methods* **9**, 357-359, doi:10.1038/nmeth.1923 (2012).
110 Humburg, P., Helliwell, C. A., Bulger, D. & Stone, G. ChIPseqR: analysis of ChIP-seq experiments. *BMC Bioinformatics* **12**, 39, doi:10.1186/1471-2105-12-39 (2011).
111 TxDb.Mmusculus.UCSC.mm10.knownGene: Annotation package for TxDb object(s) v. 3.4.7 (Bioconductor 2019).
112 Kent, W. J. *et al.* The Human Genome Browser at UCSC. *Genome Research* **12**, 996-1006, doi:10.1101/gr.229102 (2002).
113 Rosenbloom, K. R. *et al.* ENCODE whole-genome data in the UCSC Genome Browser. *Nucleic Acids Research* **38**, D620-D625, doi:10.1093/nar/gkp961 (2010).
114 Haeussler, M. *et al.* Navigating protected genomics data with UCSC Genome Browser in a Box. *Bioinformatics* **31**, 764-766, doi:10.1093/bioinformatics/btu712 (2014).
115 ggpubr: 'ggplot2' Based Publication Ready Plots (CRAN, 2020).

Supplemental Figure 1

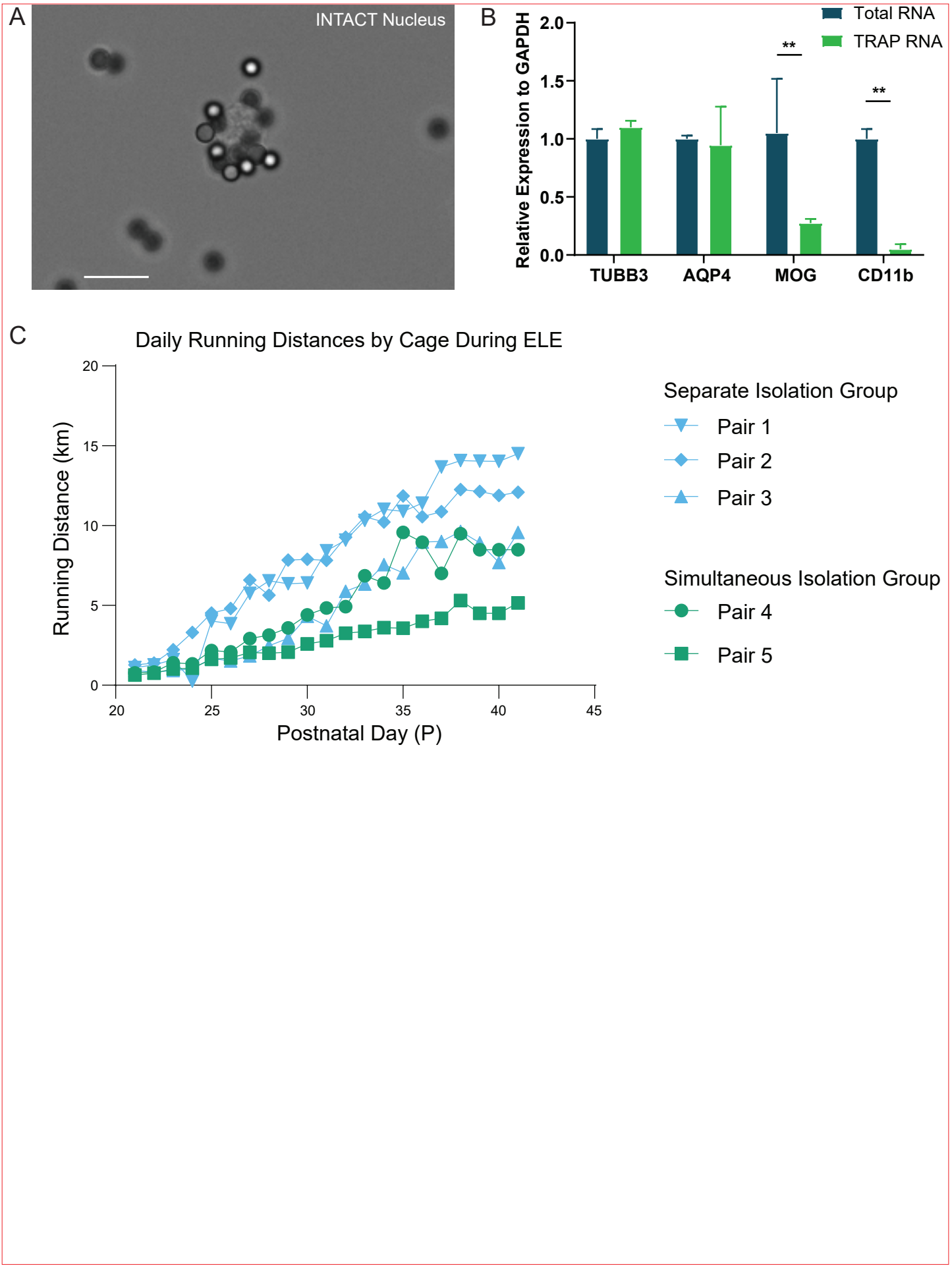

Supplemental Figure 2

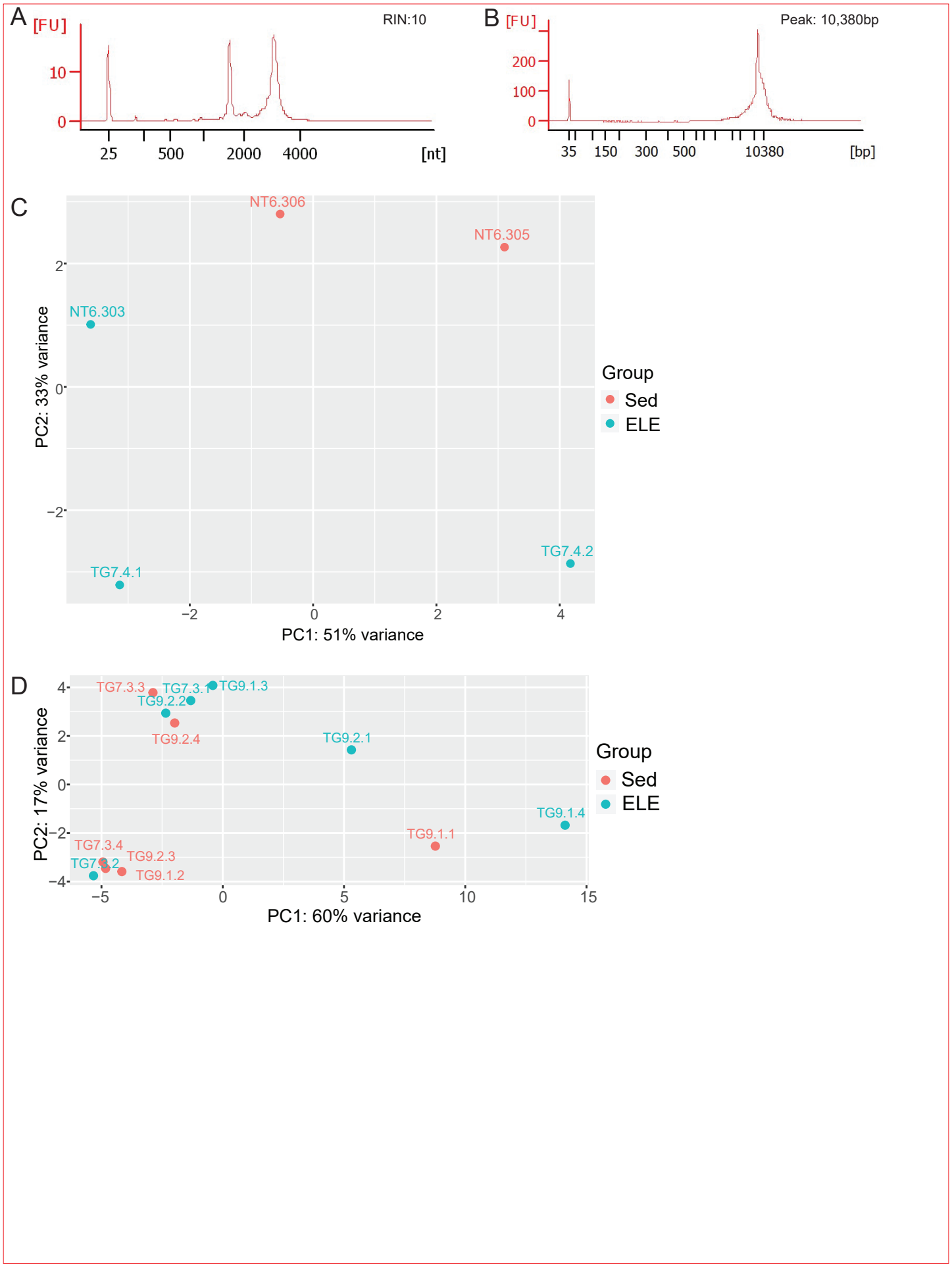
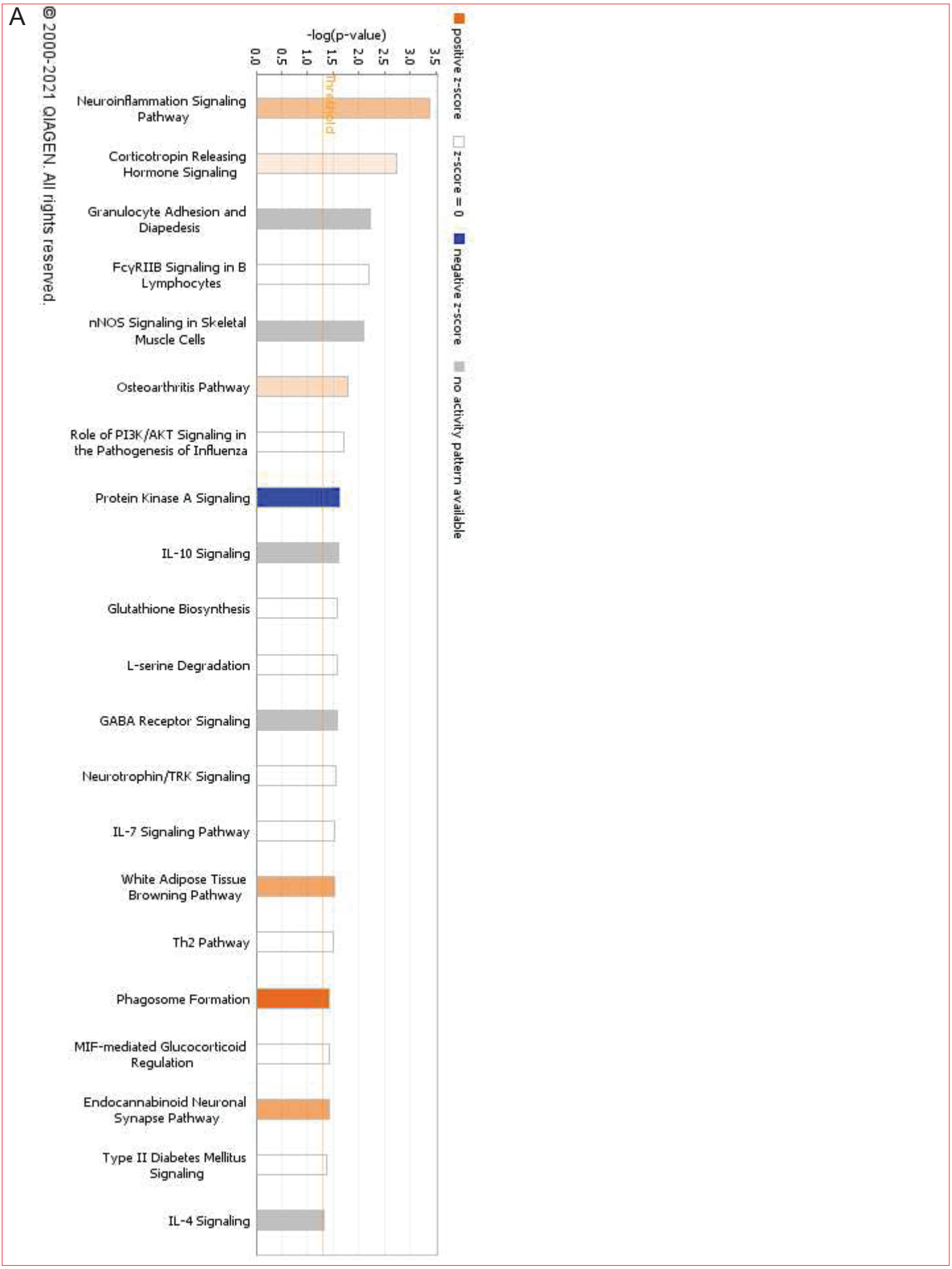
Supplemental Figure 3